The impact of alkenone degradation on $U_{37}^{K'}$ paleothermometry: a model-derived assessment

Felipe S. Freitas [1, 2, 3], Richard D. Pancost [1, 3], Sandra Arndt [2, 3, 4]

[1] Organic Geochemistry Unit, School of Chemistry, University of Bristol, Bristol, BS8 1TS, UK

[2] BRIDGE, School of Geographical Sciences, University of Bristol, Bristol, BS8 1SS, UK

[3] The Cabot Institute, University of Bristol, Bristol, BS8 1UJ, UK

[4] Department of Geosciences, Environment and Society, Université Libre de Bruxelles, Bruxelles 1050, Belgium

Corresponding author: Felipe S. Freitas (felipe.salesdefreitas@bristol.ac.uk; +44(0)1173317244)

Key Points:

- Reaction-Transport modelling shows that selective degradation of alkenones can positively bias SST records
- SST records are only likely to be affected if alkenones experience extensive degradation during burial
- The majority of alkenone-based SST records are unlikely to be affected by post-burial selective degradation

Abstract

The $U_{37}^{K\prime}$ proxy for past sea surface temperature (SST) is based on the unsaturation ratio of C_{37} alkenones. It is considered a diagenetically robust proxy, but biases have been invoked because the index can be altered by preferential degradation of the $C_{37:3}$ alkenone, resulting in higher reconstructed SST. However, alkenone degradation rate constants are poorly constrained, making it difficult to evaluate the plausibility of such a bias. Therefore, we quantitatively assessed the effect of: (1) different alkenone degradation rate constants; (2) differential degradation factors between di- and tri-unsaturated C_{37} alkenones; (3) and initial $U_{37}^{K\prime}$ values on the $U_{37}^{K\prime}$ paleothermometer for two depositional environments (shelf and upper-slope), by means of a Reaction-Transport Model (RTM). RTM results reveal that preferential degradation of $C_{37:3}$ can potentially alter the original signal of the $U_{37}^{K\prime}$ paleothermometer, but SST biases (ΔSST) are largely within $U_{37}^{K\prime}$ calibration error (ΔSST < 1.5 ºC) assuming realistic model parameters. The magnitude of ΔSST is largely determined by the degradation rate constant, but it also increases with higher differential degradation factors. Additionally, initial $U_{37}^{K\prime}$ values exert a non-linear influence on the extent of potential SST bias, with mid-range values ($0.4 < U_{37}^{K\prime} < 0.6$) being most sensitive. The most significant changes occur in the shallowest sediment layers and are attenuated with burial time/depth. Scenarios where ΔSST > 1.5 ºC are associated with marked downcore decreases in alkenone concentration. Consequently, we caution against the interpretation of $U_{37}^{K\prime}$ indices when extensive degradation results in very low alkenone concentrations (< 5 ng g^{-1}).

Key-words: Sea surface temperature; reaction-transport model; paleoceanography; paleoclimate; $U_{37}^{K\prime}$ paleothermometer, preferential degradation.

1 Introduction

Alkenones are long chain unsaturated ketones (C_{36}-C_{39}; di-, tri-, or tetra-unsaturated) that were first detected in marine sediments by *Boon et al.* [1978] and then systematically identified by *de Leeuw et al.* [1980] and *Volkman et al.* [1980b]. In the present day ocean, the modern biological precursor of these compounds are reticulofenestrid haptophytes, such as *Emiliania huxleyi* and *Gephyrocapsa oceanica* [*Volkman et al.*, 1980a, 1980b, 1995; *Marlowe et al.*, 1990; *Conte and Eglinton*, 1993; *Volkman*, 2000]. Although the occurrence of alkenones extends to the Cretaceous period [*Farrimond et al.*, 1986; *Brassell and Dumitrescu*, 2004], the presence of alkenones in Cretaceous sediments is uncommon and restricted to di-unsaturated alkenones, possibly because the $C_{37:3}$ metabolic pathway only developed in response to long-term global cooling [*Brassell*, 2014]. The oldest observed tri-unsaturated alkenones occur in early Eocene sediments, but even then they are relatively uncommon [*Marlowe et al.*, 1984; *Weller and Stein*, 2008; *Brassell*, 2014].

Crucially, numerous studies have revealed a relationship between the degree of unsaturation of C_{37} alkenones ($C_{37:2}$, $C_{37:3}$, and $C_{37:4}$; Figure 1) and algae growth temperature, resulting in the development of the U^{K}_{37} index as a proxy for sea surface temperature [*Brassell et al.*, 1986]. However, because $C_{37:4}$ alkenone concentrations are typically low (or zero) [*Grimalt et al.*, 2000] and display a high variability in relative abundance and geographic distribution across ocean basins, as well as a poor correlation with SST [*Rosell-Melé et al.*, 1994; *Sikes et al.*, 1997; *Sikes and Sicre*, 2002; *Bendle and Rosell-Melé*, 2004], *Prahl and Wakeham* [1987] and *Prahl et al.* [1988] proposed the now more widely used $U^{K\prime}_{37}$ (Eq. 1) index based on the concentrations of $C_{37:3}$ and $C_{37:2}$ alkenones:

$$U^{K\prime}_{37} = \frac{[C37{:}2]}{[C37{:}2]+[C37{:}3]} \qquad \text{(Equation 1).}$$

The quantitative relationship between the $U^{K'}_{37}$ index and ambient growth temperature has been calibrated on the basis of laboratory cultures, as well as on suspended particulate organic matter and sediment coretops [*Prahl and Wakeham*, 1987; *Müller et al.*, 1998].

Alkenones are usually well preserved in the sedimentary record [*Sikes et al.*, 1991; *Prahl et al.*, 2000]. As such, the $U^{K'}_{37}$ paleothermometer is considered diagenetically robust (*i.e.* resistant and/or little altered during diagenesis) and is extensively used to reconstruct past ocean and lake surface temperature [*Prahl et al.*, 2000, 2003; *Ho et al.*, 2013; *Brassell*, 2014]. Consequently, the validity of the proxy relies on the assumptions that alkenones are relatively recalcitrant and, more importantly, that all C_{37} alkenones degrade at similar rates. However, several studies have shown that alkenones can be rapidly degraded in the water column, in marine sediments, and under laboratory conditions [*Conte et al.*, 1992; *Freeman and Wakeham*, 1992; *Hoefs et al.*, 1998; *Teece et al.*, 1998; *Gong and Hollander*, 1999; *Rontani et al.*, 2005, 2008; *Rontani and Wakeham*, 2008; *Huguet et al.*, 2009]. In addition, unsaturated lipids are generally considered more easily degradable than saturated compounds [*Volkman et al.*, 1983; *Cranwell et al.*, 1987; *Grimalt et al.*, 2000], and different alkenones might thus be degraded at different rates.

However, there is conflicting evidence regarding the question whether there is a preferential degradation of $C_{37:3}$ over $C_{37:2}$ alkenones. Several studies found no evidence for preferential degradation [*e.g.*, *Prahl et al.* 1989, 2000, 2003; *Sikes et al.* 1991; *Conte et al.* 1992; *Rontani et al.* 1997; *Teece et al.* 1998; *Grimalt et al.* 2000; *Herbert*, 2001], whereas others directly observed or inferred a higher degradation of the $C_{37:3}$ alkenone [*Freeman and Wakeham*, 1992; *Hoefs et al.*, 1998; *Gong and Hollander*, 1999; *Rontani et al.*, 2005, 2008, 2013; *Huguet et al.*, 2009]. Their observations indicate that the potential bias in reconstructed SST induced by such a preferential degradation ranges from 0 to up to +5.9 ºC under both oxic and anoxic conditions and in both in the water column and sediments [*Rontani et al.*, 2013].

Regardless of the main drivers of preferential degradation, a potential diagenetic modification of the primary signal could have important implications for paleoreconstructions and could result in erroneous conclusions. For instance, many Paleogene sediments only contain the $C_{37:2}$ alkenone [*e.g., Marlowe et al.* 1984; *Pagani et al.*, 1999, 2000; *Mercer and Zhao*, 2004; *Lyle et al.*, 2006]. These observations could be interpreted as a high SST during the Paleogene or could be the result of preferential degradation of the $C_{37:3}$ alkenone. Much of the scientific debate has revolved around the existence of preferential degradation and its potential controls, whereas little attention has been devoted to quantitatively assessing the potential influence of preferential degradation on the downcore profiles of $C_{37:2}$ and $C_{37:3}$ and thus, the evolution of the $U_{37}^{K\prime}$ ratio during burial. Such an assessment would not only advance our understanding of the possible impacts of preferential degradation on the $U_{37}^{K\prime}$ derived paleoreconstructions, but could also help identify the range of conditions (*e.g.* sedimentation rate, concentrations, degradation rate constants) under which preferential degradation could compromise the applicability of the $U_{37}^{K\prime}$ paleothermometer. Furthermore, it could help disentangle the interplay between preferential degradation and additional processes that can induce SST biases, such as resuspension and lateral transport [*e.g., Benthien and Müller,* 2000; *Ohkouchi et al.,* 2002; *Mollenhauer et al.,* 2003].

However, alkenone degradation rate constants are poorly constrained, making it difficult to quantitatively assess the influence of preferential degradation on $U_{37}^{K\prime}$ derived paleoreconstructions. In addition, extrapolating experimental results of alkenone degradation to geological timescales, especially over a large range of environmental conditions, is not straightforward. Therefore, here we use a reaction-transport model (RTM) approach [*Berner*, 1980; *Boudreau*, 1997] to quantitatively assess the potential impact of preferential degradation on the $U_{37}^{K\prime}$ paleothermometer during burial in marine sediments. The specific aims of this work are to: (1) quantitatively assess the impact of preferential degradation on $U_{37}^{K\prime}$

paleothermometry; (2) identify the main factors that control SST biases and quantify their relative significance; and (3) based on the model results, evaluate the impact of preferential degradation on the application of the $U_{37}^{K\prime}$ paleothermometer. With respect to the latter, we revisit previously published data but our goal is not to recalculate published SSTs; rather it is to explore the implications of our sensitivity experiment for such records and provide a guide for critical assessment of the $U_{37}^{K\prime}$ proxy in future studies.

2 Model Description

The RTM approach allows the simultaneous tracking of alkenone concentrations and the sedimentary $U_{37}^{K\prime}$ indices in a given sediment layer during burial in marine sediments. Additionally, model simulations enable an evaluation and comparison of short- and long-term impacts. Here, we first provide a detailed description of the modelling approach. The model is then used to explore the evolution of the $U_{37}^{K\prime}$ ratio during burial for different environmental conditions (depositional environments with distinct sediment accumulation rates and bioturbation coefficients), $U_{37}^{K\prime}$ initial values, and alkenone degradation parameters (degradation rate constant and differential degradation factor between alkenones). We develop a comprehensive sensitivity study that allows us to explore the full range of these parameters, given their poorly constrained nature, in order to establish a quantitative framework for understanding the conditions under which $U_{37}^{K\prime}$ indices could have been biased. The model developed here is based on the vertically-resolved mass conservation equation for alkenones in marine sediments (Eq. 2) [*e.g.*, *Berner*, 1980]:

$$\frac{\partial C_{37:i}}{\partial t} = -\frac{\partial F_i}{\partial z} + \sum_j R_i^j \quad \text{(Equation 2)},$$

where $C_{37:i}$ is the concentration of alkenone *i*, *z* is the sediment depth, *t* denotes the time, F_i summarizes the advective and dispersive flux divergence of alkenone *i* and $\sum_j R_i^j$ represents

143 the sum of production/consumption rates *j* that affect alkenone *i*. This approach allows the
144 evolution of alkenone concentration to be explored with both burial time and burial depths.
145 Burial depth and time are directly linked via the characteristic timescales of transport processes
146 F_i *(i.e.* in a non-compacting sediment, burial time $t=z/w$*)*. Figure 2 shows a conceptual
147 illustration of the alkenone degradation model applied here and the following sections provide
148 a detailed model description.

149 The model accounts for the advective burial flux of alkenones, as well as the random
150 displacement of sediments caused by the activity of infaunal organisms in the bioturbated zone
151 of the sediment ($z < z_{bio}$), which is described as a dispersive process [*Boudreau*, 1986] with a
152 constant bioturbation coefficient D_{bio}. The bioturbation coefficient is set to zero below the
153 bioturbated zone. In addition, alkenones are consumed by heterotrophic degradation during
154 burial. The degradation of organic compounds is a multi-step process. However, the initial
155 hydrolysis step is considered to be the rate limiting step and the degradation process is thus
156 generally described as a single step reaction following first order kinetics [*e.g., Arnosti,* 2011].
157 Traditionally, organic matter reactivity and thus, the reaction rate constant or reactivity, *k*, of
158 the kinetic rate law is assumed to be controlled by the molecular structure of the organic
159 compound [*e.g.*, Rechka and Maxwell, 1988; Sun and Wakeham, 1994]. In this case, the
160 susceptibility of alkenone $C_{37:i}$ towards microbial degradation would not change during burial
161 and its degradation can thus be described by a constant reactivity k_i. The resulting rate law is
162 equivalent to the so-called 1G Model [*e.g.*, *Boudreau* 1997]. However, some empirically
163 determined k_i values from pelagic environments and shallow oxic sediments are extremely
164 high. For instance, *Gong and Hollander* [1999] determined rate constants of $k_i \approx 10^{-3}$ yr^{-1} for
165 sediments from the Santa Monica Basin, and *Freeman and Wakeham* [1992] and *Sun and*
166 *Wakeham* [1994] measured a value of $k_i = 9.0 \cdot 10^{-3}$ yr^{-1} in sediments from the Black Sea. If
167 applied in a 1G model, such high rate constants would result in a complete alkenone

consumption within the upper sediment layer and thus, contradict the observed persistence of alkenones in marine sediments, suggesting that these rate constants are not representative or that alkenone reactivity might decrease with depth/time. Indeed, observations have shown that the reactivity of organic matter is not only controlled by its chemical structure. Organic matter reactivity results from the interplay between the organic matter and its environment, and consequently is not a characteristic attributed solely to organic matter itself [*Mayer*, 1995]. Therefore, the reactivity of the C_{37} alkenones could, in addition to their molecular structures, also be controlled by factors such as the macromolecular structure in which the compounds are incorporated, oxygen exposure time and terminal electron acceptor availability, microbial community structure, physical protection, and priming [*e.g., Aller,* 1994; *Keil et al.,* 2004; *Burdige,* 2006; *Zonneveld et al.,* 2010; *Arndt et al.,* 2013]. In fact, observational evidence indicates that the degradation of lipids, amino acids, carbohydrates, as well as of bulk organic carbon is more similar within a depositional setting than the degradation of individual compounds across sites [*e.g., Burdige,* 2006]. This suggests that alkenones degrade similarly as bulk organic matter and that additional environmental controls could cause a decrease in apparent alkenone reactivity during burial. Several studies support this hypothesis. They show that additional factors, such as oxygen exposure times [*e.g., Gong and Hollander,* 1999] and microbial community dynamics [*e.g., Rontani et al.,* 2008], can exert an influence on the apparent reactivity of alkenones, causing *k* to decrease during burial. Such a decrease in reactivity can be mathematically described by a power law, equivalent to the widely used reactive continuum (RCM) and power models of organic matter degradation [*Middelburg,* 1989; *Boudreau and Ruddick,* 1991]. Here, we developed two reactivity scenarios to test the influence of preferential degradation on changes in SST assuming (1) a constant alkenone reactivity with burial depth (1G model), based on the classical view of a chemical structure controlled degradation, and (2) a decreasing alkenone reactivity with burial depth (power

model/reactive continuum model), based on observational evidence for additional controls on apparent alkenone reactivity.

Scenario 1: Constant reactivity, k_i, during burial (1G model) (Eq. 3-4):

Assuming a constant reactivity, k_i, the vertically-resolved mass conservation equation for alkenone concentrations, $C_{37:i}$, in marine sediments can be formulated as:

$$\frac{\partial C_{37:i}}{\partial t} = D_{bio}\frac{\partial^2 C_{37:i}}{\partial z^2} + \omega\frac{\partial C_{37:i}}{\partial z} - k_i C_{37:i} \text{ for } z < z_{bio} \quad \text{(Equation 3)}$$

$$\frac{\partial C_{37:i}}{\partial t} = \omega\frac{\partial C_{37:i}}{\partial z} - k_i C_{37:i} \text{ for } z \geq z_{bio} \quad \text{(Equation 4),}$$

where $C_{37:i}$ represents the alkenone ($C_{37:2}$ or $C_{37:3}$) concentration at depth, D_{bio} denotes the bioturbation diffusion coefficient, ω is the burial velocity, and k_i is the first order degradation rate constant for alkenone $C_{37:i}$. A preferential degradation factor $f_{C37:3}$ relates the degradation rate constants k_i of $C_{37:3}$ and $C_{37:2}$ alkenones and thus, serves as a quantitative measure of the extent of preferential degradation:

$$k_{37:3} = f_{C37:3}.k_{37:2} \quad \text{(Equation 5).}$$

Scenario 2: Decreasing reactivity, $k_i(z)$, during burial (Reactive Continuum Scenario) (Eq. 6-7):

A decrease in alkenone reactivity during burial can be mathematically described by a power law and is equivalent to the widely used reactive continuum (RCM) and power models of organic matter degradation [*Middelburg*, 1989; *Boudreau and Ruddick*, 1991]. Assuming a decreasing reactivity, $k_i(z)$, the vertically-resolved mass conservation equation for alkenone concentrations, $C_{37:i}$, in marine sediments is then given by:

$$\frac{\partial C_{37:i}}{\partial t} = D_{bio}\frac{\partial^2 C_{37:i}}{\partial z^2} + \omega\frac{\partial C_{37:i}}{\partial z} - k_i(z) C_{37:i} \text{ for } z < z_{bio} \quad \text{(Equation 6)}$$

$$\frac{\partial C_{37:i}}{\partial t} = \omega \frac{\partial C_{37:i}}{\partial z} - k_i(z) C_{37:i} \quad \text{for } z \geq z_{bio} \text{ (Equation 7),}$$

where the decrease in $k_i(z)$ with sediment burial age, *burial time(z)*, is described in the form of the power law relationship [*Middelburg*, 1989; *Boudreau and Ruddick*, 1991]:

$$k_i(z) = \frac{p_i}{a_i + burial\ time(z)} \text{ (Equation 8),}$$

where p_i and a_i are parameters that determine the depth profile of k_i. The a_i parameter denotes the apparent initial age of the alkenone mixture in the sediment and can be seen as a shape parameter, whereas the p_i parameter scales the initial distribution of alkenones [*Boudreau and Ruddick*, 1991]. Low a_i and high p_i represent a dominance of more bioavailable alkenones, whereas high a_i and low p_i represent a dominance of less bioavailable alkenones. Therefore, the apparent alkenone reactivity in the upper sediment layers will be higher for low a_i values (more bioavailable alkenones), which results in a rapid loss of alkenones at surface sediments, but also a rapid decrease in $k_i(z)$ with depth. Alternatively, high a_i values will yield lower apparent alkenone reactivity close to the sediment-water interface (less bioavailable alkenones); consequently, alkenones will have lower degradability at surface sediments and the downcore decrease in $k_i(z)$ will be slower [see *Arndt et al.*, 2013 Fig. 10 for details]. In the case of the RCM, the preferential degradation factor $f_{C37:3}$ could in theory be applied to both the a_i and p_i parameter. The parameter p_i merely scales the reactivity of alkenones. The application of the preferential degradation factor $f_{C37:3}$ to p_i according to

$$p_{37:3} = f_{C37:3} \cdot p_{37:2} \text{ (Equation 9)}$$

results in a shift of the entire reactivity profile $k_i(z)$ for tri-saturated alkenones to higher reactivity and is identical to its use in Scenario 1. It is important to note that, in this case, the 1G model represents an end-member RCM scenario, *i.e.* no decrease of alkenone reactivity with burial time/depth and therefore, can be considered as a 'worst case' scenario for a preferential degradation bias.

We can further assume a different decrease in reactivity with burial between the two alkenones. In this case, a preferential degradation arises from a difference in a_i values ($C_{37:3}$ more labile than $C_{37:2}$, *i.e.* $a_{37:3} << a_{37:2}$) and, thus, the preferential degradation factor would be applied to a_i. Such assumption, however, would suggest that the two alkenones have distinct sources, undergo different transport mechanisms, and/or are differently affected by mineral protection, microbial community dynamics or terminal electron acceptor availability before/during burial. Those assumptions seem unlikely, and if true, would prevent the application of $U_{37}^{K'}$ as a SST proxy. Therefore, we generally assume that the parameter a_i, which controls the shape of the reactivity decrease with depth, is identical for both alkenones. Nonetheless, we also tested this hypothesis to assess the potential SST biases that could arise from such conditions.

2.1 Solution

Equations 3-4 and 6-7 can be used to trace the evolution of alkenone concentrations in a given sediment layer during burial by assuming steady state conditions ($\frac{\partial C}{\partial t} = 0$) and a constant porosity, thus neglecting sediment compaction. In addition, we also assume that benthic activity efficiently mixes material in the bioturbated layer, resulting in a constant age. Burial time (*i.e.* the age of a given sediment layer) and burial depth, *z*, are then related by:

$$burial\ time(z) = 0 \text{ for } z < z_{bio} \text{ (Equation 10),}$$

$$burial\ time(z) = \frac{z - z_{bio}}{\omega} \text{ for } z \geq z_{bio} \text{ (Equation 11).}$$

The integration of Eqs. 3-4 and 6-7 can then be solved analytically and yield the following general solutions representing the evolution of alkenone concentrations with burial depth/time:

Scenario 1: Constant reactivity, k_i, during burial (1G Scenario) (Eq. 3-4):

$$C_{37:i}(z) = A_1 e^{a_1 \cdot z} + B_1 e^{b_1 \cdot z} \text{ for } z < z_{bio} \quad \text{(Equation 12)}$$

$$C_{37:i}(z) = A_2 e^{a_2 \cdot z} \text{ for } z \geq z_{bio} \quad \text{(Equation 13)}$$

where:

$$a_1 = \frac{\omega - \sqrt{\omega^2 + 4 \cdot D_{bio} \cdot ki}}{2 \cdot D_{bio}} \quad \text{(Equation 14)}$$

$$b_1 = \frac{\omega + \sqrt{\omega^2 + 4 \cdot D_{bio} \cdot ki}}{2 \cdot D_{bio}} \quad \text{(Equation 15)}$$

$$a_2 = \frac{-ki}{\omega} \quad \text{(Equation 16)}$$

Determining the integration constants A1, B1 and A2 requires the definition of boundary conditions. Here, we assume:

(1) a known concentration of the alkenones at the sediment water interface

$C_{37:i}(0) = C_{37:i,0}$ (Equation 17);

and (2 and 3) continuity between the bioturbated and non-bioturbated zone:

(2) $C_{37:i,1}(z_{bio}) = C_{37:i,2}(z_{bio})$ (Equation 18);

(3) $D_{bio} \cdot \frac{\partial C_{z_{bio}}}{\partial z} | zbio = 0$ (Equation 19).

Scenario 2: Decreasing reactivity, $k_i(z)$, during burial (Eq. 5-6; RCM Scenario):

$$C_{37:i}(z) = A_1 e^{a_1 \cdot z} + B_1 e^{b_1 \cdot z} \text{ for } z < z_{bio} \quad \text{(Equation 20)}$$

$$C_{37:i}(z) = C_{37:i}(z_{bio}) . \left(\frac{a_i}{a_i + burial\ time(z)}\right)^{-p_i} \text{ for } z \geq z_{bio} \quad \text{(Equation 21)}$$

where:

$$a_1 = \frac{\omega - \sqrt{\omega^2 + 4 \cdot D_{bio} \cdot p_i / a_i}}{2 \cdot D_{bio}} \quad \text{(Equation 22)}$$

$$b_1 = \frac{\omega + \sqrt{\omega^2 + 4 \cdot D_{bio} \cdot p_i/a_i}}{2 \cdot D_{bio}}$$ (Equation 23)

Eq. 6 is thus mathematically equivalent to Eq. 3 with reactivity $k_i(z) = {}^{p_i}/_{a_i}$ (Equation 24), within the bioturbated layer.

Determining the integration constants A1, B1 requires the definition of boundary conditions. Here, we assume:

(1) a known alkenone concentration at the sediment water interface

$C_{37:i}(0) = C_{37:i,0}$ (Equation 25);

(2) continuity between the bioturbated and non-bioturbated zone:

(2) $D_{bio} \cdot \frac{\partial C_{z_{bio}}}{\partial z} | zbio = 0$ (Equation 26).

2.2 Model Parameters and Boundary Conditions

Model parameters and boundary conditions place the model in its environmental context. Table 1 provides an overview of the respective model parameters and boundary conditions, their units and their values. Model parameters can be divided into those that define the general depositional environment and are generally well constrained, and those that control alkenone degradation and are generally variable and/or poorly constrained. Therefore, a two-step sensitivity study is conducted here. Model simulations are carried out for two different depositional environments (coastal sediments – water depth 200 meters; and upper slope sediments – water depth 1000 meters) to explore their potential impact on preferential degradation and the $U_{37}^{K'}$ paleothermometer. In addition, for each depositional setting, a sensitivity study is conducted over the entire range of plausible degradation parameters to account for the parameter uncertainty of degradation parameters.

2.2.1 Sensitivity to Depositional Environment

In marine sediments, burial depth and time are directly linked via the characteristic timescales of transport processes (Eq. 10-11) and, thus, the bioturbation coefficient, bioturbation depth and burial velocity. The model calculates the alkenone concentration depth profiles for both a typical coastal sediment, as well as an upper slope sediment up to a maximum sediment column depth of 250 meters.

Based on a compilation of mixing layer depths [*Boudreau*, 1994, 1998], the depth of the bioturbated zone is set to 10 cm for both water depth scenarios. Bioturbation coefficients and burial velocities are determined based on a water depth dependent relationship proposed by *Middelburg et al.* [1997]. This approach aims at providing a general framework for potential alkenone bias with burial time/depth for contrasting depositional environments rather than simulating any specific setting. Note that, since the model traces the evolution of alkenone layers during burial, (likely) changes in sedimentation rate over burial time would merely have an impact on the calculation of burial depth (Eq. 11). For instance, a decrease in sedimentation rate would simply reduce burial depth for a given burial time, but would not have an impact on the simulated SST bias and, thus, the overall results. Although C_{37} alkenone concentrations at the sediment water interface (SWI) can be highly variable depending on local primary production rates and vertical transport in the water column, sediment trap and surface sediment studies [*Gong and Hollander*, 1999; *Müller and Fischer*, 2001; *Prahl et al.*, 2001; *Rodrigo-Gámiz et al.*, 2016] indicate that alkenone concentrations in settling suspended matter and surface sediments typically range from approx. 4 – 77 µg g^{-1}. Thus, the total C_{37} alkenone ($C_{37:2}$ + $C_{37:3}$) concentration at the SWI was set to 5 µg g^{-1}.

335 *2.2.2 Sensitivity to Uncertainty in Degradation Rate Parameters*

336 Most of the parameters that control the potential degree of preferential degradation (such as the
337 initial $U_{37}^{K\prime}$ of the material that has been deposited at SWI, $U_{37}^{K\prime}(0)$; the degradation rate
338 constant, k_i; and the differential degradation factor between di- and tri-unsaturated C_{37}
339 alkenones, $f_{C37:3}$) are either variable and/or difficult to constrain. Therefore, we designed a
340 comprehensive parameter sensitivity study in order to assess the response of alkenone
341 concentration depth profiles and thus, the $U_{37}^{K\prime}$ ratio to different degrees of preferential
342 degradation. The evolution of alkenone concentrations with burial time/depth is thus simulated
343 over the entire plausible parameter range of: i) the initial $U_{37}^{K\prime}$, $U_{37}^{K\prime}(0)$; ii) the degradation rate
344 constant, k_i; and iii) the differential degradation factor between di- and tri-unsaturated C_{37}
345 alkenones, $f_{C37:3}$.

346 The $U_{37}^{K\prime}(0)$ was varied over the entire range of 0.1 to 0.9 $U_{37}^{K\prime}$ units only excluding $U_{37}^{K\prime}$
347 = 0 and $U_{37}^{K\prime}$ = 1, reflecting the absence of $C_{37:2}$ and $C_{37:3}$, respectively. Degradation rate
348 constants, k_i, are notoriously difficult to constrain. First order rate constants derived from
349 laboratory experiments [*Teece et al.*, 1998] are often not directly transferable to marine
350 sediments characterized by low or no oxygen exposure, low temperature and high pressure
351 [*Schouten et al.*, 2010] and estimates from the field are highly variable [*e.g., Sun and Wakeham,*
352 1994; *Gong and Hollander,* 1999]. Therefore, we do not rely on these rate constant values;
353 instead, we explore the entire range of potential values. However, we do interpret the model
354 results in the context of these experimental and field estimates (see *Section 4.1).* Model-derived
355 first-order degradation rate constants of bulk organic matter typically vary by several orders of
356 magnitude, from as high as 10^{1} yr^{-1} to as low as 10^{-9} yr^{-1} [*Arndt et al.*, 2013]. Therefore, we
357 vary the first order degradation rate constant k_i from 10^{-5} to 10^{-3} yr^{-1} (1G model). The lower
358 limit is set to 10^{-5} yr^{-1}, because lower degradation rate constants result in a negligible effect of
359 preferential degradation on $U_{37}^{K\prime}$; as such, this study represents a 'worst case scenario' for $U_{37}^{K\prime}$

bias. The upper limit is defined as 10^{-3} yr^{-1}, because levels higher than that seem unrealistic, since they result in complete consumption of alkenones in the sediment surface layer.

Similar to constant first order degradation rate constants, the free parameters *p* and *a* that control the shape of the $k_i(z)$ depth profile are also difficult to constrain. Model-derived parameters from a wide range of different environments indicate that *p* generally falls within the range between 10^{-2} and 10^{0}, while the parameter *a* may vary over several orders of magnitude from 10^{-1} to 10^{6} yrs [*Arndt et al.*, 2013]. Here, the free parameter a_i varies from 10^{-1} to 10^{4} yrs, whereas p_i varies from 10^{-2} to 10^{0}. We, therefore, explore the entire range of plausible degradation rate constants for both the 1G model and the RCM scenario.

To simulate the preferential degradation of tri-unsaturated alkenones, a ratio between the $C_{37:3}$ degradation rate constant and the $C_{37:2}$ degradation rate constant – a preferential degradation factor $f_{C37:3}$ – is defined and varied from 1.1 to 1.5 (*i.e.* $C_{37:3}$ degradation is 10% to 50% faster than the degradation of $C_{37:2}$). This range has been informed by observed differences of preferential alkenones degradation in field and laboratory experiments [*e.g.*, *Hoefs et al.*, 1998; *Gong and Hollander*, 1999; *Rontani et al.*, 2005, 2008].

2.3 Model Output

The model calculates the evolution of individual alkenone concentrations over burial time/depth (Eq. 3-4 and 6-7). Based on these simulated concentrations, $U_{37}^{K\prime}$ ratios are calculated according to Eq. 1. SSTs are estimated based on the calculated $U_{37}^{K\prime}$ ratios using the global core-top calibration of *Müller et al.* [1998] (Table 1). SST is calculated from the SWI down to 250 meter below sea floor (mbsf) for the parameter combinations described in Table 1. The deviation of the estimated SST from the original SST recorded by the material deposited at the sediment-water interface or, in other words, the SST bias due to preferential degradation (ΔSST; Table 1) is calculated for typical burial depths 50, 100, 150, 200, and 250 mbsf. For

385 the hypothetical coastal sediments (200 meters depth), those depths represent burial times of
386 approximately 14 kyr, 28 kyr, 42 kyr, 55 kyr, and 70 kyr, respectively. For the hypothetical
387 upper slope sediments (1000 meters depth), those depths correspond to 31 kyr, 62 kyr, 94 kyr,
388 125 kyr, and 156 kyr, respectively.

389

390 **3 Results**

391 In the following sections, we mainly focus on the findings derived from the 1G approach
392 (Figures 3 – 6; Table 2) or, in other words, the 'worst case' endmember RCM scenario
393 (negligible decrease in k_i with depth/time) described in Section 2.2. We do so because that
394 approach results in the most extensive degradation and, thus, SST bias. As such, simulation
395 results will help to delineate a conservative range of conditions that favor preferential
396 degradation and potentially result in SST bias. The discussion of the 1G – 'worst case' RCM –
397 simulation results are supplemented with simulation results from Scenario 2 (Figures 7 – 10),
398 in which we test a broad range of a_i and p_i values.

399 Figures 3 to 6 summarize changes in the $U_{37}^{K\prime}$ derived SSTs and alkenone concentrations
400 as a function of all parameters explored in the Scenario 1. To illustrate the effect of preferential
401 degradation on ΔSST (*i.e.* the deviation from the real SST) for a wide range of degradation
402 scenarios and environmental conditions, interpolated plots of simulated ΔSST over the
403 simulated $U_{37}^{K'}(0)$ and $f_{C37:3}$ space are produced for each water depth (Fig. 3-6 a and b, two
404 columns: 200 m and 1000 m), different burial depths/times (Fig. 3-6 a and b, 5 panels per
405 column: 50 mbsf, 100 mbsf, 150 mbsf, 200 mbsf and 250 mbsf), and degradation rate constants
406 (Fig. 3-6). The simulated burial depths represent sediment ages ranging from 14 kyr to 70 kyr
407 and from 31 kyr to 156 kyr for the shallow and deep site, respectively. In addition, vertical
408 profiles of the preserved fraction of the original deposited total alkenone ($C_{37:2}$+$C_{37:3}$)
409 concentration over burial depth/time are plotted to visualize the decrease in total alkenone

410 concentrations (Fig. 3-6 c and d). Furthermore, Table 2 summarizes the range of ΔSST values
411 and C_{37} alkenone extent of degradation throughout all scenarios explored in Scenario 1.

412 The 1G simulations (Fig. 3-6) show that the impact of preferential degradation on $U_{37}^{K\prime}$
413 ratios and, thus, the positive bias in reconstructed SST ranges from less than 0.1 ºC in the least
414 reactive and/or least selective degradation scenario ($k_{37:2} = 1.0 \cdot 10^{-5}$ yr^{-1}; $f_{C37:3} = 1.1$; $U_{37}^{K'}(0) =$
415 0.1 and 0.9) up to 27 ºC in the most extreme ($k_{37:2} > 1.0 \cdot 10^{-4}$ yr^{-1}; $f_{C37:3} > 1.4$; $U_{37}^{K'}(0) = 0.1$),
416 albeit unrealistic (see below), scenario (Table 2; Figures 3 to 6). In general, the influence of
417 preferential degradation on the bias in reconstructed SST is controlled by a combination of
418 factors. The most important factors are the degradation rate constants k_i, the initial $U_{37}^{K'}(0)$
419 value and the preferential degradation factor $f_{C37:3}$, while water depth (and thus, the general
420 depositional environment) exerts an important but subordinate impact. In addition, the lower
421 panels c and d (Fig. 3-6) illustrate the dramatic influence of increasing degradation rate
422 constants, k_i, on alkenone concentrations and their downcore preservation. For example, when
423 k_i is assumed to be $1.0 \cdot 10^{-4}$ yr^{-1}, then less than 1% of the originally deposited alkenones are
424 preserved at a burial depth of 50 mbsf.

425 In general, ΔSST increases with an increase in alkenone degradation rate constants, k_i,
426 and preferential degradation factor, $f_{C37:3}$. An extremely high k_i ($1.0 \cdot 10^{-3}$ year^{-1}) yields a large
427 ΔSST (~ 27 ºC) and extensive loss of C_{37} alkenone (>> 99.9%, results not shown). Yet, such
428 an extreme distortion of the $U_{37}^{K\prime}$ seems unlikely, given the fact that alkenones are generally
429 well preserved, even in highly oxidising sediments [*e.g.*, *Prahl et al.*, 1989, 2003]. Lower k_i
430 values ($k_i < 2.5 \cdot 10^{-5}$ year^{-1}) result in lower alkenone degradation rates (fraction degraded at
431 250 mbsf is < 99%) and, thus, represent more plausible scenarios. In addition, Fig. 3-6 show
432 that maximum ΔSST is generally observed for mid-range $U_{37}^{K'}(0)$, and ΔSST is smaller when
433 initial $U_{37}^{K\prime}(0)$ values are low or high (Fig. 3). This is especially true for high indices ($U_{37}^{K\prime}(0) >$
434 0.8), which, of course, have a limited capacity to increase further. Even low initial $U_{37}^{K\prime}(0)$

values are relatively robust under low degradation scenarios (Fig. 3). However, an increase in alkenone degradation, due to higher degradation rate constants (Fig. 5-6) and/or water and burial depths (a-b), shifts the ΔSST maximum from mid $U_{37}^{K'}(0)$ values towards lower $U_{37}^{K'}(0)$ values ($U_{37}^{K'}(0) < 0.2$) (Figure 6).

Similar to Scenario 1 (constant reactivity, k_i), Scenario 2 simulations (RCM approach, decreasing reactivity with burial time/depth, $k_i(z)$) can be assessed in the context of all parameters summarized in Table 1. Figures 7 and 8 illustrate changes in the $U_{37}^{K'}$ derived SSTs and alkenone concentrations for each depositional environment and assuming $a_i = 10^0$ yr and $a_i = 10^3$ yr, respectively, and $p_i = 10^{-1}$ (see above for figure details).

As already pointed out in section 2, a decrease in degradation rate constant k_i results in generally lower SST biases over the considered burial times. For higher initial alkenone reactivity ($a_i = 10^0$ yr), ΔSST does not exceed 6 ºC (Figure 7), and ΔSST < 2 ºC for less reactive, but slowly decreasing alkenone reactivity ($a_i = 10^3$ yr; Figure 8). Similar to Scenario 1, SST bias increases with an increase in preferential degradation factor ($f_{C37:3}$), and the maximum ΔSST is generally observed for the mid-range $U_{37}^{K'}(0)$ values and decreases when $U_{37}^{K'}(0)$ values are either low or high. Unlike Scenario 1 (constant reactivity), the most significant changes occur in the upper sediment layers and ΔSST, as well as the degree of loss of alkenones (Figure 7-8, c-d) becomes attenuated with burial time/depth, due to the decrease in reactivity ($k_i(z)$). Figure 9 illustrates the decrease in $k_i(z)$ with burial time/depth, assuming $p_i = 10^{-1}$ for $a_i = 10^0$ yr (Figure 9a) and $a_i = 10^3$ yr (Figure 9b). The lower a_i value results in a higher reactivity ($k_i(0) \approx 10^{-1}$ yr^{-1}) close to the sediment-water interface. However, $k_i(z)$ decreases quickly in the upper sediment layers to $k_i(z) < 10^{-5}$ yr^{-1} at 50 mbsf and only decreases very slowly with increasing burial time/depth. The higher a_i value results in a lower reactivity ($k_i(0) \approx 10^{-4}$ yr^{-1}) close to the sediment-water interface, but decreases very slowly with burial time/depth. However, at greater burial depth, where burial time $t >> a_i$, alkenone reactivity approaches

similar values as for lower a_i values ($k_i(z) < 10^{-5}$ yr^{-1}) because Eq. 8 becomes dominated by burial time instead of a_i. Thus, even with distinct $k_i(0)$, increasing burial time/depth yields similar $k_i(z)$-values and these change much slowly than those of upper sediment layers. The rapid decrease in $k_i(z)$ means that the degradation induced bias in SST is small and generally does not exceed the $U_{37}^{K'}$ calibration error. In detail, high a_i values (Fig. 9b) reflect an overall low reactivity and yield a slow downcore decrease in $k_i(z)$, resulting in minor changes in SST (Fig. 8). The largest ΔSST (~ 6 ºC) are generally associated with low a_i value ($a_i = 10^{-1}$ yr) and high preferential degradation factors $f_{C37:3} = 1.5$ (Fig. 7). Such low a_i values produce the most dramatic decrease in $k_i(z)$ with depth (Fig. 9a) and, thus, represent the most heterogeneous distribution of alkenone reactivity.

Although unlikely, we can also explore the impact of differential evolution of alkenone reactivity with burial time, *i.e.* assuming different a_i values for the di- and tri-unsaturated alkenone pools ($C_{37:3}$ more labile than $C_{37:2}$). Figure 10 presents the simulated evolution of $k_i(z)$ and SST with burial time/depth, assuming an initially high but rapidly decreasing reactivity for the $C_{37:3}$ pool ($a_{C37:3} = 0.1$ yr) and an initially low but slowly decreasing reactivity for the $C_{37:2}$ pool ($a_{C37:2} = 100$ yrs). This represents an extreme case scenario, since it assumes a large difference in the evolution of the reactivity with burial depth/time (Fig. 10a). The degradation rate constant $k_{C37:3}$ is three order of magnitude higher than $k_{C37:2}$ in the surface sediments. The rate constants then decrease at different rates with burial depth, before reaching similar magnitudes in deeper sediment layers (> 50 mbsf). Fig. 10b shows that the largest SST changes occur in the shallowest sediment layers, with the most pronounced ΔSST (> 10 ºC) for $U_{37}^{K'}(0)$ < 0.5. Deeper in the sediment, degradation rates and SST biases significantly slow down.

Overall, the decrease in $k_i(z)$ with burial time/depth (Scenario 2) could explain the discrepancy between the fast degradation rates observed in laboratory experiments [*Teece et al.*, 1998; *Rontani et al.*, 2005, 2008], as well as field observations [*Sun and Wakeham*, 1994;

Gong and Hollander, 1999] and the long-term persistence of alkenones in the geological record [*Brassell*, 2014]. In addition, simulation results indicate that Scenario 2 (decrease in $k_i(z)$ with burial time/depth) generally results in limited SST biases often below the detection limit. In contrast, Scenario 1 (constant k_i) results in more pronounced SST bias and thus, serves as 'worst case' endmember scenario and provides a conservative framework to further investigate SST bias. The following sections assess the role of different controls on preferential alkenone degradation in altering $U_{37}^{K'}$ during burial and thus, inducing biases in reconstructed SSTs.

4 Discussion

4.1 Disentangling the controls on SST bias during burial

Overall, both 1G (Scenario 1) and RCM (Scenario 2) simulations indicate that the following three factors control the magnitude of diagenetic modification on $U_{37}^{K'}$ indices: 1) the extent of alkenone degradation, which, in turn, is controlled by the degradation rate constant, k_i, the burial depth, z, and the water depth; 2) the initial $U_{37}^{K'}$ value, $U_{37}^{K'}(0)$; and 3) the preferential degradation factor, $f_{C37:3}$. It is important to note that the influence of these three factors on ΔSST is tightly linked. For instance, the extent of degradation exerts no impact on ΔSST if there is no preferential degradation and vice versa. We also note that our simulations include scenarios in which intense alkenone degradation results in concentrations below the detection limit (< 5 ng g^{-1}), *i.e.* situations where $U_{37}^{K'}$ could not be determined. Therefore, for the remainder of the discussion we only consider model results in which > 0.1% of the original alkenone concentration is preserved.

4.1.1 Extent of degradation

Scenarios 1 and 2 reveal that the extent of degradation – as a cumulative effect of k_i, as well as water and burial depths/time – is the major control on ΔSST. The positive bias in $U_{37}^{K'}$ generally increases with an increasing extent of degradation during burial (Fig. 3-8).

The alkenone degradation rate constant, k_i, exerts an important control on the extent of degradation. The reconstructed ΔSST increases from < 0.1 ºC to up to 27 ºC with an increase in degradation rate from $1.0 \cdot 10^{-5}$ yr^{-1} to $1.0 \cdot 10^{-4}$ yr^{-1} (Fig. 3-6). This is particularly critical as alkenone degradation rate constants are difficult to constrain and also implicitly account for factors that control alkenone degradation during burial, but are not explicitly accounted for in the model [*Arndt et al.*, 2013]. Of all k_i values assessed in the present RTM study, $k_i < 1.0 \cdot 10^{-5}$ yr^{-1} seems to best represent the reactivity of alkenones in the sedimentary archive. This refers not only to SST biases (ΔSST < 6.0 ºC), but also to the amounts of alkenones degraded. The adoption of faster, and constant, k_i (*e.g.* $k_i > 5.0 \cdot 10^{-5}$ $year^{-1}$) results in an almost complete degradation of alkenones (>> 99.9%), which is inconsistent with their apparent persistence in the sedimentary record [*Brassell*, 2014]. However, experimentally derived k_i values obtained by *Teece et al.* [1998] for $C_{37:3}$ are four orders of magnitude higher than what we infer to be our most realistic values, if those values are assumed to be constant with burial time/depth. Similarly, *Rontani et al.* [2005, 2008] also report k_i values in the order of 10^{-1} yr^{-1} for alkenones in degradation laboratory experiments. However, these rate constants were derived from fresh alkenone material in laboratory incubations, where conditions were optimized to investigate alkenone degradation. This experimental setting could result in a 'priming effect' and enhance the degradation of more recalcitrant material [*Aller*, 1994; *Aller and Blair*, 2006]. Therefore, they do not account for the complexity of natural conditions [*Schouten et al.*, 2010], and it seems likely that these experiments represent unrealistically high degradation rates compared to natural settings. Environmental conditions that likely account for the lower degradation rates

include changes in terminal electrons availability (TEA) (*e.g.* O_2 availability) and/or packing in macromolecular complexes or mineral particles, which would slow down or prevent microbial attack [see *Arndt et al.*, 2013 and references therein for overview].

The extent of alkenone degradation in sediments also depends on water and burial depths/times and thus, the physical depositional environment, which exerts a positive, albeit secondary control. Alkenones deposited in deeper waters experience a greater degree of degradation at similar burial depths, due to slower burial rates or in other words longer burial times [*Middelburg et al.*, 1997]. This effect is consistent with observational data. *Conte et al.* [1992] observed a rapid and significant (by 1-2 orders of magnitude) degradation of alkenones in deep North Pacific waters. In particular, burial depth and, thus, burial time controls the extent of degradation. Longer burial time (*i.e*. deeper depths in the sediment) allows for a longer exposure of alkenones to heterotrophic degradation, therefore resulting in more intensive degradation and ultimately a stronger bias in SST. This becomes evident in Fig 3-6 (Scenario 1). Assuming the least dramatic condition (Fig. 3), the maximum perturbation in SST increases from < 2 ºC at 50 mbsf to up to 6 ºC at 250 mbsf. Alternatively, scenarios with higher k_i values (Fig. 6), yield ΔSST of 10 ºC at 50 mbsf and 27 ºC at 250 m. Although unrealistic, the latter illustrates how burial depth, as a component of extent of degradation, controls SST biases. However, in Scenario 2, burial time/depth becomes less important with time/depth (Fig. 7-8), due to the decrease of $k_i(z)$ (Fig. 9). In fact, under such conditions, $k_i(z)$ and SST bias become attenuated at greater depths.

4.1.2 The initial $U_{37}^{K\prime}$ value

Initial $U_{37}^{K\prime}$ values at the SWI ($U_{37}^{K\prime}(0)$) exert a non-linear effect on ΔSST during burial and mid-range values ($U_{37}^{K\prime}i \approx 0.5$) generally exhibit the most pronounced SST bias (Fig. 3-4 and 7-8). As *Hoefs et al.* [1998] previously pointed out, such a result is mathematically expected and is

560 the likely explanation for the disagreement between experimental alkenone degradation
561 studies. Under similar conditions, *Rontani et al.* [1997] and *Teece et al.* [1998] found no
562 significant degradation-induced changes in $U_{37}^{K\prime}$, whereas *Rontani et al.* [2005] later observed
563 a positive degradation-induced bias of 0.1 $U_{37}^{K\prime}$ units. *Rontani et al.* [2005] argued that the
564 different outcome of these degradation experiments can be explained by different initial $U_{37}^{K\prime}$
565 values: 0.49 in *Rontani et al.* [2005]; 0.75 in *Teece et al.* [1998]; and 0.85 in *Rontani et al.*
566 [1997]. Model results confirm that $U_{37}^{K\prime}$ values are relatively robust towards preferential
567 degradation for both high and low $U_{37}^{K'}(0)$ when the extent of degradation is low (low k_i,
568 shallow sediment depth/short burial times; Fig. 3-4 and 7-8). However, low $U_{37}^{K'}(0)$ initial
569 conditions become more sensitive to diagenetic alteration under intense degradation scenarios
570 (high k_i, low sedimentation rate, deep burial depth/ long burial times), and maximum ΔSST
571 shifts to low $U_{37}^{K'}(0)$ under such conditions (Fig 5-6).

572 The combined effects of degradation extent and $U_{37}^{K'}(0)$ are illustrated in Fig. 11. This
573 shows how the extent of degradation exerts a first order control on ΔSST, with $U_{37}^{K'}(0)$ exerting
574 a lesser and non-linear SST bias. Moreover, $U_{37}^{K'}(0)$ = 0.5 is most prone to SST biases when
575 degradation is low and lower values of $U_{37}^{K'}(0)$ are more prone to SST biases when degradation
576 is extensive.

577

578 *4.1.3 Preferential degradation factor*

579 The preferential degradation factor $f_{C37:3}$ is the parameter that ultimately controls the difference
580 between the degradation rates of the di- and tri-unsaturated C_{37} alkenones. Regardless of the
581 environmental triggers for C_{37} selective degradation (see Introduction), RTM results show that
582 an increase in $f_{C37:3}$ and thus, a more pronounced preferential degradation of $C_{37:3}$ generally
583 leads to a pronounced increase in ΔSST (Figure 3-8). However, the sensitivity of $U_{37}^{K\prime}$ and ΔSST

584 to an increase in $f_{C37:3}$ depends on the extent of degradation and thus, the degradation rate
585 constant k_i. Even high $f_{C37:3}$ values of 1.5 only induce small ΔSSTs unless the degradation rate
586 constant is large.

587 Additionally, the impact of $f_{C37:3}$ on ΔSST is also dependent on the $U_{37}^{K'}(0)$. As
588 previously pointed out, ΔSST is mostly affected when $U_{37}^{K'}(0)$ = 0.5 and the extent of
589 degradation is low. Thus, the preferential degradation factor $f_{C37:3}$ most impacts mid-range
590 values of $U_{37}^{K'}(0)$. Figure 12, assuming a constant degradation rate (*e.g.* $k_i = 5 \cdot 10^{-5}$ yr^{-1}), allows
591 us to explore the effects of $f_{C37:3}$ and $U_{37}^{K'}(0)$ on ΔSST. For the lowest $f_{C37:3}$ = 1.1 (Fig. 12a),
592 the change in SST shows a linear downcore trend; the $U_{37}^{K'}(0)$ = 0.5 yields the largest SST
593 perturbation, whereas the high-end $U_{37}^{K'}(0)$ value is the least altered. Increasing the preferential
594 degradation factor to $f_{C37:3}$ = 1.2 (Fig. 12b) and $f_{C37:3}$ =1.3 (Fig. 12c) results in a non-linear
595 ΔSST, as well as a shift towards maximum ΔSST occurring at lower $U_{37}^{K'}(0)$ values. These
596 results arise because increasing $f_{C37:3}$ values results in preferential loss of $C_{37:3}$ alkenone and
597 therefore, stronger biases at the lower-end of $U_{37}^{K'}(0)$. Overall and as expected, it is clear that
598 $f_{C37:3}$ exerts a direct control on SST biases. However, only high $f_{C37:3}$ values in combination
599 with intense degradation rates (*i.e.* high k_i) induce ΔSST larger than the $U_{37}^{K'}$ calibration error.
600 Model results emphasize the need to better constrain $f_{C37:3}$ values in natural settings and to
601 identify the factors that control the preferential degradation of $C_{37:3}$. Laboratory incubation
602 experiments performed by *Teece et al.* [1998] found negligible differences in $C_{37:2}$ and $C_{37:3}$
603 alkenone degradation rates, yielding $f_{C37:3} \approx 1.0$. Later experiments conducted by *Rontani et al.*
604 [2008] were able to produce up to 3 ºC positive SST biases; given that $U_{37}^{K'}(0) > 0.7$ in that
605 study, a 3 ºC ΔSST yields $f_{C37:3} \sim 1.2$. Similar analyses can be conducted for field studies (Table
606 3) and explain apparently contradictory behavior. For example, at the Peruvian Margin,
607 *McCaffrey et al.* [1990] found an alkenone loss of 30% in the top 1 cm of sediments underlying

anoxic waters, but $U_{37}^{K\prime}$ was largely unaffected. Our model results show that when $f_{C37:3} < 1.5$, the extent of degradation must exceed 50% to yield measurable ΔSST. *Prahl et al.* [1989, 2003] observed extensive loss of alkenones in the Madeira Abyssal Plain (MAP) turbidites (86 – 99%), but only minor changes in $U_{37}^{K\prime}$ indices (ΔSST < 1.3 ºC for $U_{37}^{K\prime}(0) \geq 0.7$). Model results indicate that this requires a preferential degradation factor $f_{C37:3}$ between 1.1 and 1.2 for the MAP turbidites. *Hoefs et al.* [1998] reported a > 99% extent of degradation associated with a +0.17 increase in $U_{37}^{K\prime}$ indices (*i.e.* ΔSST ~ 5ºC), which yields an $f_{C37:3} \sim 1.3$ in our simulations. There is also evidence that $f_{C37:3}$ differs between oxic and anoxic settings. In the Santa Monica Basin sediments, *Gong and Hollander* [1999] compared $U_{37}^{K\prime}$ records from two adjacent areas and observed a difference in reconstructed SST of up to 4 ºC, with oxic settings recording higher temperatures than anoxic ones. However, the extent of degradation was 60% for both settings, indicating that $f_{C37:3}$ differed between the two, being ~1.3 and ~1.0 in the oxic and anoxic settings (assuming no preferential degradation at the anoxic setting), respectively.

Preferential degradation under aerobic conditions [*Hoefs et al.*, 1998; *Gong and Hollander*, 1999] has been attributed to preferential degradation of the tri-unsaturated $C_{37:3}$ alkenone via double bond epoxidation [*Rontani et al.*, 2008]. This process occurs more effectively at position ω29, only present on the $C_{37:3}$ alkenone, rather than positions ω15 and ω22 which occur on both C_{37} alkenones, and is suggested to be mediated by the bacterial strain *Dietzia maris* sp. S1 [*Rontani and Wakeham*, 2008; *Zabeti et al.*, 2010]. Despite this, it appears that aerobic microbially-mediated selective degradation occurs in a non-systematic way [*Rontani et al.*, 2005, 2008; *Rontani and Wakeham*, 2008], which compromises our ability to quantify and predict its controls on preferential degradation in marine sediments. Moreover, as discussed above, $f_{C37:3}$ appears to be consistently greater than 1 in a variety of settings such that it cannot be solely dependent on oxic/anoxic conditions [*Rontani and Wakeham*, 2008].

633 *4.2 Implications for $U_{37}^{K'}$ paleothermometry*

634 Our model exploration of alkenone degradation provides a quantitative framework for
635 assessing SST reconstructions. Here, we illustrate how model results can be used to explore or
636 offer alternative explanations for SST mismatches in the sedimentary archive.

637 First, the magnitude of SST bias will depend on the initial $U_{37}^{K'}$ value. As previously
638 discussed (Section 4.1.2), high $U_{37}^{K'}$ values are least affected, implying that the alkenone-
639 derived SST records from relatively warm settings will have been less affected than those from
640 colder settings [*e.g.*, *Rodrigo-Gámiz et al.*, 2016].

641 Second, the extent of degradation exerts a very strong control on SST reconstructions.
642 The *Müller et al.* [1998] SST calibration is characterized by a standard error of ±1.5 ºC, and
643 preferential $C_{37:3}$ degradation that produces biases > 1.5 ºC are thus of particular concern.
644 Although previous studies argued that ΔSST > 1.5 ºC warm biases do occur [*Madureira et al.*,
645 1995; *Hoefs et al.*, 1998; *Gong and Hollander*, 1999; *Pagani et al.*, 1999], model results show
646 that if the extent of alkenone degradation is low (< 50%), such biases require a high preferential
647 degradation factor, *i.e.* $f_{C37:3} \geq 1.5$ (Figure 11). This scenario seems unrealistic since it assumes
648 a $C_{37:3}$ degradation rate that is at least 50% faster than $C_{37:2}$. It is also inconsistent with most
649 experimental and field investigations (see above). Yet, if the extent of degradation is high (50
650 to 99.9%), SST biases > 1.5 ºC are simulated for $f_{C37:3}$ values ranging from 1.1 to 1.4. In the
651 most extreme degradation scenario (> 99.9%), any $f_{C37:3} > 1.0$ can produce SST biases above
652 1.5 ºC (Fig. 11). However, as already pointed out, such high degradation rates significantly
653 reduce alkenone concentrations, rendering the analytical determination of $U_{37}^{K'}$ ratios
654 challenging. In fact, SST biases can also arise from instrumental errors when concentrations
655 are extremely low [*Grimalt et al.*, 2000, 2001].

656 Overall and holding other factors equal, reconstructed SSTs are most biased in older
657 sediments, where the extent of degradation will be most severe for a given depositional setting.

Although this is valid for both scenarios, in Scenario 2 (decrease in $k_i(z)$ with burial time/depth), degradation rapidly slows down in very old/deeply buried sediments and differences in SST bias thus become negligible when comparing sediment layers/burial times $t >> a_i$. Model results reveal how several mathematical factors mitigate and exacerbate that effect. Assuming steady state, degradation is most rapid in shallow sediments and slows with depth, an effect exacerbated in Scenario 2. In contrast, the impact of degradation on $U_{37}^{K\prime}$ increases as degradation approaches its mathematical limit (*i.e.* 100%). These two factors work in tandem. Therefore, we would expect ΔSST biases to occur throughout the burial time and from the entire sediment column rather than solely in deep sediments. Therefore, it is useful to evaluate $U_{37}^{K\prime}$-derived SST records against those based on other proxies in both recent and older sediment records.

4.2.1 Assessing potential degradation bias in recent sedimentary records

In general, alkenone-derived SST estimates agree well with other SST reconstructions for shallow geological time periods (< 500 kyrs), indicating that diagenetic alterations of the $U_{37}^{K\prime}$ paleothermometer are negligible. For example, $U_{37}^{K\prime}$ and Mg/Ca (*Globigerinoides sacculifer*) SSTs estimates from the Western Equatorial Pacific (WEP) are of a similar magnitude over the past 30 kyr [*de Garidel-Thoron et al.*, 2007]. This was observed despite relatively low alkenone concentrations and possibly extensive degradation, suggesting that preferential degradation had only a minor impact (*i.e.* $f_{C37:3} \approx 1.0$). The glycerol dialkyl glycerol tetraether (GDGT)-based TEX_{86} (tetraether index of tetraethers consisting of 86 carbons) proxy [*Schouten et al.*, 2002] is a widely used organic paleothermometer [*e.g., Schouten et al.,* 2013] which also exhibits a close agreement with $U_{37}^{K\prime}$-derived SSTs over shallow timescales. For example, $U_{37}^{K\prime}$ and TEX_{86} SST estimates obtained from core tops within the Arabian Sea (NIOP905 and 74KL) match modern mean annual SST values for that area [*Huguet et al.,* 2006]. In the Eastern

683 Mediterranean (GeoB7702-3), $U_{37}^{K'}$ and TEX_{86} also record similar trends and absolute SST
684 values over the past 27 kyr [*Castañeda et al.*, 2010]. $U_{37}^{K'}$ and TEX_{86}-based reconstructions
685 agreed well even in depth intervals where alkenone concentrations were low, indicating that
686 even a high extent of degradation did not alter the $U_{37}^{K'}$ signal at these sites. In the Western
687 Mediterranean, *Huguet et al.* [2011] reported similar temperature trends between $U_{37}^{K'}$ and
688 TEX_{86} for the last 244 – 130 kyrs. Although, TEX_{86} absolute SST were higher than $U_{37}^{K'}$ SST,
689 the difference rarely exceeded < 3 ºC, which is within both proxy calibration errors (and
690 inconsistent with the latter being biased to warm temperatures). In fact, in many cases where
691 TEX_{86} and $U_{37}^{K'}$ -derived SSTs differ, it is due to the latter being colder rather than warmer
692 [*Huguet et al.*, 2006; *Castañeda et al.*, 2010; *Grauel et al.*, 2013]; and in the few settings where
693 the opposite is observed [*Lopes dos Santos et al.*, 2010; *McClymont et al.*, 2012; *Seki et al.*,
694 2012; *Li et al.*, 2013], it is often attributed to the depth of GDGT production.
695
696 *4.2.2 Assessing potential degradation bias in older sedimentary records*
697 In general, inferred degradation biases have been largely limited to deep time (Miocene and
698 older) settings. For instance, the absence of tri-unsaturated alkenone in many Miocene
699 sediments from DSDP (Deep Sea Drilling Program) sites 588, 608 and 730 results in $U_{37}^{K'}$ values
700 of 1 and therefore, SST > 28 ºC [*Pagani et al.*, 1999]. RTM results suggest that these
701 observations might indicate long-term preferential consumption of $C_{37:3}$ – and indeed alkenone
702 concentrations are low in these sediments. However, such a scenario would require extensive
703 degradation and, although mathematically possible, remains inconsistent with the lack of such
704 extensive degradation in younger settings. Therefore, we suggest, based on insights gained
705 through the model investigation, that at the DSDP sites 588, 608 and 730 Miocene SST records
706 have not been extensively affected by selective degradation and that SSTs were indeed
707 relatively high. It is worth noting that one rationale for those suggestions was the much higher

temperatures recorded by alkenones than by planktonic foraminifera $\delta^{18}O$. However, those isotopic records have almost certainly been biased by diagenetic recrystallization [*e.g., Pearson et al.*, 2001, 2007], and these records have now been discarded [*Pagani et al.*, 2010]. This illustrates some of the challenges associated with multi-proxy SST reconstructions and the pitfalls of interpreting proxies with preconceived notions of relative fidelity.

In Paleogene sediments, more complex temperature relationships have been observed, with offsets between $U_{37}^{K'}$ and foraminiferal $\delta^{18}O$-derived SSTs ranging from 0 to 10 ºC [*Pagani et al.*, 2005; *Liu et al.*, 2009]. Again, this could be due to a long-term selective degradation of alkenones or diagenetic alteration of foraminifera $\delta^{18}O$ values [*Pearson et al.*, 2001, 2007; *Pagani et al.*, 2010]. Our RTM results support the latter, because such significant SST bias at such high $U_{37}^{K'}$ indices is difficult to achieve without nearly complete degradative loss of the alkenones.

Nonetheless, we do acknowledge that in some settings large SST off-sets between alkenones and other proxies are observed and more difficult to explain. For example, *Weller and Stein* [2008] observed that $U_{37}^{K'}$-derived SSTs in the Eocene Arctic Ocean were up to 10 ºC higher than the TEX_{86}-derived SSTs reported by *Brinkhuis et al.* [2006]. A recent re-analysis of TEX_{86}^{H}-derived temperatures suggests that the offset between TEX_{86}^{H} and $U_{37}^{K'}$ in deep-time settings could result from a calibration bias [*Ho and Laepple*, 2016]; however, if this assumption is valid that would yield higher TEX_{86}^{H} SSTs. *Weller and Stein* [2008] argued that the observed offset arises from the distinct ecological characteristics of alkenone and GDGT producers, as they likely occupy different habitats in the water column. This seems likely because model results, although showing that preferential degradation of $C_{37:3}$ can yield 10 ºC offsets, show that this can only happen under extreme degradation conditions.

The RTM approach applied here illustrates how such interpretations can be tested in more than simply an *ad hoc* manner when reconstructed SSTs are perceived to be too high,

particularly when looking at absolute SST values, since SST differences (relative values) are expected to be less biased. In particular, reconstructed SSTs should be interpreted in the context of the most important factors that could potentially drive putative SST biases: the presumed initial $U_{37}^{K'}(0)$ value and the extent of alkenone degradation. RTM results allow exploring the robustness of relative temperature changes resulting from contrasting $U_{37}^{K'}(0)$ by shifting temperature changes (higher SST shifted minimally, whereas lower SST shifted more strongly).

4. Conclusions

RTM simulations show that preferential degradation of tri- over di-unsaturated C_{37} alkenone can potentially alter the original signal of the $U_{37}^{K'}$ paleothermometry and consequently produce positively biased SST records. Results from a plethora of environmental and degradation scenarios indicate that a combination of factors can results in a large range of possible SST biases, but the greatest changes require extensive alkenone degradation. Positively biased SST records are also governed by the differential degradation factor between C_{37} alkenones ($f_{C37:3}$), which based on various modern studies appears to vary between 1 and 1.5; however, these extreme values seem limited to only some settings. Initial $U_{37}^{K'}(0)$ plays a secondary role on the SST changes. Not all of the simulated scenarios are realistic; those that yield maximum SST biases would require that alkenones be effectively removed from the sedimentary record – a direct consequence of the major control exerted by the degree of degradation. However, modest SST biases are associated with realistic assumptions about degradation rates, consistent with environmental studies (*i.e.* in oxidised turbidites). Consequently, we caution against the interpretation of $U_{37}^{K'}$ indices when alkenone concentrations are low, especially if low concentrations are a direct result of extensive degradation.

RTM results offer a possible complementary explanation for SST off-sets between $U_{37}^{K\prime}$ and other paleotemperature proxies found in the geological record and help elucidate mismatches between proxies. Additionally, it can be useful to avoid erroneous paleoreconstructions and interpretations derived from $U_{37}^{K\prime}$ diagenetically altered signals. Nevertheless, comparisons between our RTM results and the alkenone sedimentary record suggest that, in general, $U_{37}^{K\prime}$-SST records have not been as extensively altered as sometimes assumed.

Tables and figure captions

Table 1: Selective degradation alkenones RTM components

Parameter	Description	Value/Range	Unit
C	*$C_{37:2}$ or $C_{37:3}$ concentration at depth*		µg cm^{-3}
C_0	*$C_{37:2}$ or $C_{37:3}$ concentration at SWI*	0.5 – 4.5	µg g^{-1}
k_i	*Degradation rate constant*	10^{-5} – 10^{-3}	$year^{-1}$
a_i	*Apparent initial age*	10^{-1} – 10^{4}	year
p_i	*Shape parameter of alkenones distribution*	10^{-2} – 10^{0}	
D_{bio}	*Diffusion bioturbation coefficient*	12.05; 25.06	cm^2 $year^{-1}$
ω	*Burial velocity*	0.16; 0.36	cm $year^{-1}$
ρ	*Sediment density*	2.5	g cm^{-3}
z	*Sediment depth*	0 – 25.000	cm
z_{bio}	*Bioturbation depth*	10	cm
	Water depth	200; 1.000	m
$U_{37}^{K'}(0)$	*$U_{37}^{K'}$ initial fractionation at SWI*	0.1 – 0.9	
$f_{C37:3}$	*$C_{37:3}$ preferential degradation factor*	1.1 – 1.5	
SST	*Sea surface temperature**	$U_{37}^{K'}$ = 0.033·SST + 0.044	ºC
ΔSST	*SST excursion or bias from SWI to depth*	SST_{SWI} - SST_{Depth}	ºC

**Müller et al.* [1998];

Table 2. Sea surface temperature biases and total alkenone preservation in sediments from 50 and 250 mbsf, based on different 1G RTM scenarios

k_i (year^{-1})	Minimum ΔSST (ºC)[a]		Maximum ΔSST (ºC)[b]		Fraction of alkenone preserved (%)[b]	
	200[c]	1000[c]	200[c]	1000[c]	200[c]	1000[c]
$1.0 \cdot 10^{-5}$	0.03	0.08	2.6	5.7	48.1	20.1
$2.5 \cdot 10^{-5}$	0.09	0.20	6.4	13.5	16.6	1.9
$5.0 \cdot 10^{-5}$	0.18	0.39	12.3	22.4	2.8	0.4
$1.0 \cdot 10^{-4}$	0.35	0.74	20.8	27.1	< 0.1	< 0.1
$1.0 \cdot 10^{-3}$	2.21	2.8	27.2	27.2	<<0.1	<<0.1

[a]at 50 mbsf; [b]at 250 mbsf; [c]water depth;

821 **Table 3.** Published experimental and field derived alkenones degradation data summarizing the main preferential

822 degradation parameters

Study	Setting	$U_{37}^{K'}(0)$	ΔSST	Extent of degradation
Teece et al., 1998	Experimental[1]	0.74	< 1.0	85
	Experimental[2]	0.59	<0.1	40
Rontani et al., 2005	Experimental[1]	0.49	~ 3.0	93
	Experimental[3]	0.49	<0.1	95
Rontani et al., 2008	Experimental[1]	0.77	~ 3.0	78
McCaffrey et al., 1990	Peruvian Margin	0.7	< 0.5	30
Prahl et al., 2003	MAP - 140 ky	0.71	<0.5	86
	MAP - Late Pliocene	0.91	<0.5	95
	MAP - Early Pliocene	0.91	<0.5	98
	MAP - Late Micene	0.94	<0.5	99
Hoefs et al., 1998	MAP - Late Pliocene	0.77	0.5	>99
	MAP - Early Pliocene	0.86	2.0	>99
	MAP - Late Miocene	0.87	0.6	>99
	MAP - Middle-late Miocene	0.92	2.5	>99
Gong and Hollander, 1999	Santa Monica Basin[4]	0.54	2.5 - 4	60

823 [1]Oxic; [2]Sulphate reduction; [3]Denitrification; [4]Oxic/Anoxic; MAP – Madeira Abyssal Plain;

824

825

826

827

828

829

830

831

832

833

834

835

836

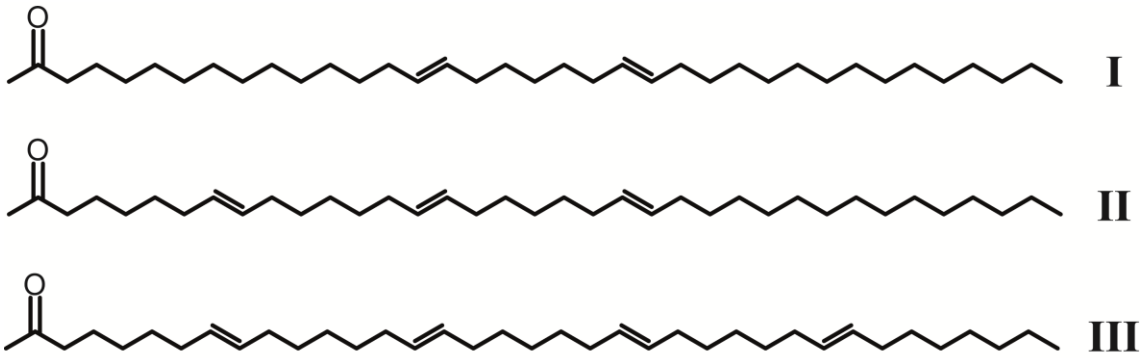

Figure 1. Chemical structure of C_{37} alkenones. (I) Heptatriaconta-8,15-dien-2-one – $C_{37:2}$; (II) Heptatriaconta-8,15,22-trien-2-one – $C_{37:3}$; (III) Heptatriaconta-8,15,22,29-tetraen-2-one – $C_{37:4}$.

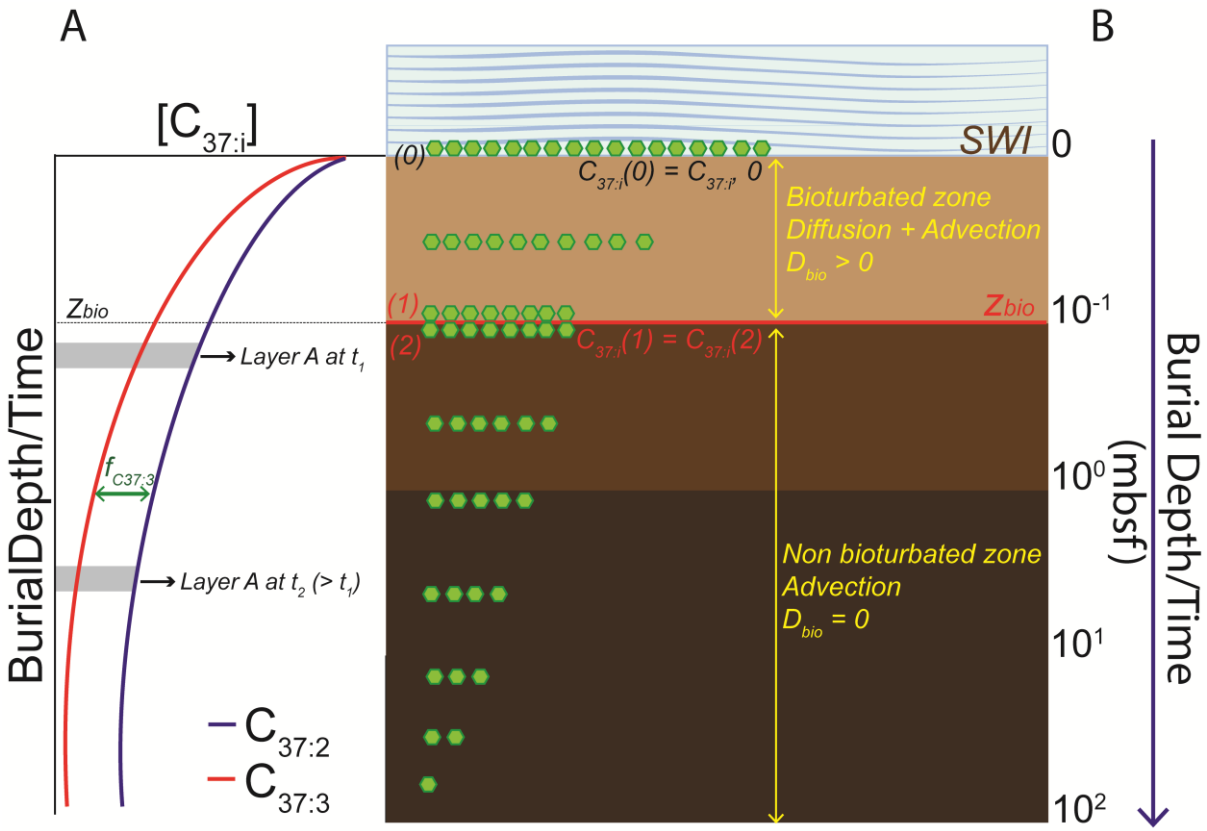

Figure 2. Schematic representation of one-dimensional alkenone degradation in marine sediments with main model elements. (a) Hypothetical downcore evolution of C_{37} alkenone concentrations ($C_{37:i}$) as a result of transport and reaction processes during burial in the sediment; the blue line represents $C_{37:2}$ alkenone concentrations, whereas the red line represents $C_{37:3}$ concentrations. The green arrow indicates the preferential degradation factor, $f_{C37:3}$, of $C_{37:3}$ over $C_{37:2}$ during selective degradation. (b) Conceptual representation of C_{37} alkenone burial and degradation as a modelled sediment column; the green hexagons represent C_{37} alkenone concentrations and the red line marks the limit of bioturbated zone (z_{bio}). D_{bio} denotes the bioturbation diffusion coefficient. SWI represents the sediment water interface.

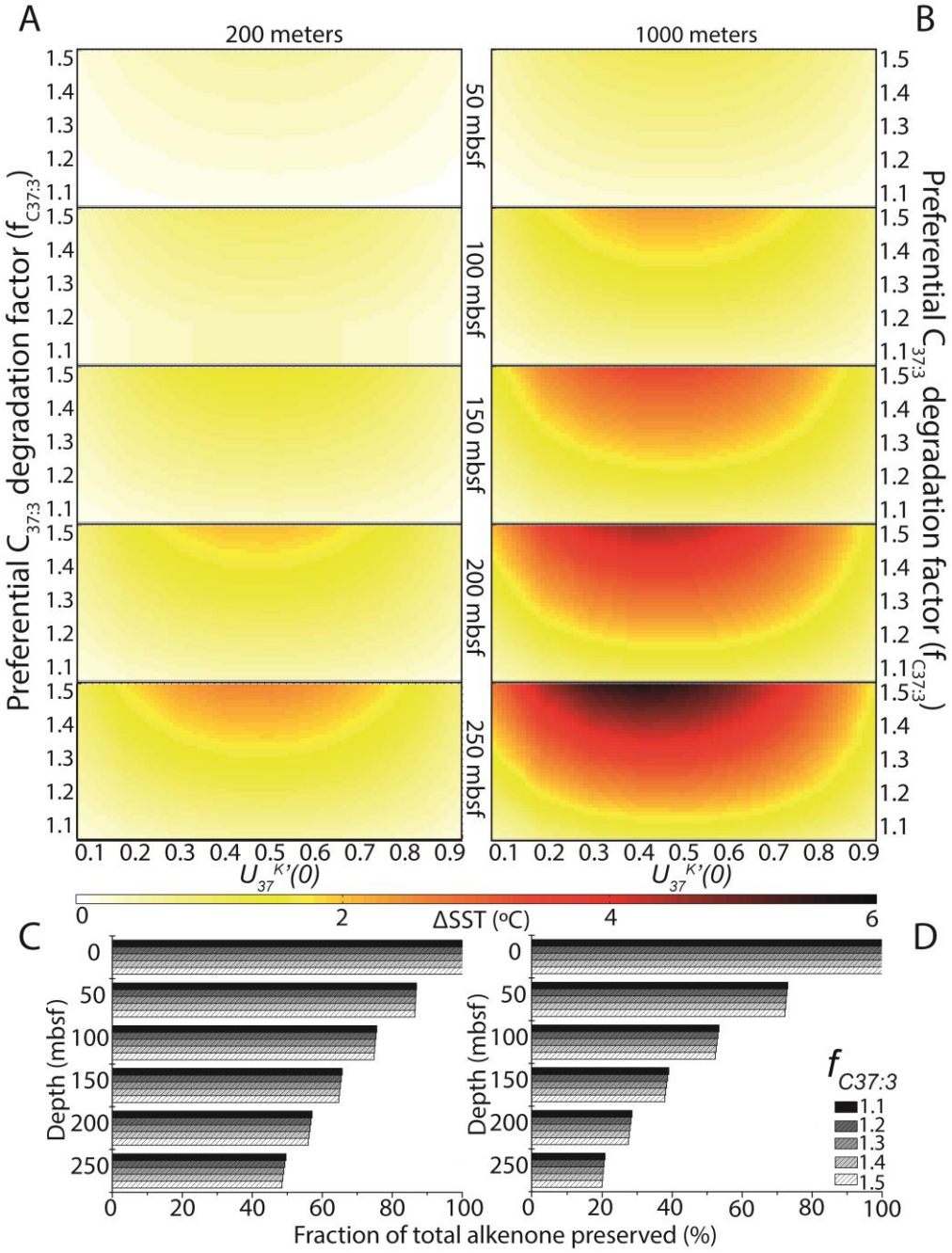

862

863 **Figure 3**. Interpolated SST positive bias and total alkenones preserved in sediment resulting from selective
864 degradation of alkenones in a 1G-RTM simulation assuming a rate constant (k_i) of $1.0 \cdot 10^{-5}$ year^{-1}. (a) Downcore
865 SST bias at 200 meters water depth; (b) Downcore SST bias at 1,000 meters water depth; (c) Downcore total
866 alkenones preserved (%) in sediment at 200 meters water depth; (d) Downcore total alkenones preserved (%) in
867 sediment at 1,000 meters water depth**.** ΔSST denotes SST at sediment-water interface (SWI) – SST at depth;
868 $U_{37}^{K'}(0)$ denotes $U_{37}^{K'}$ initial values at SWI; $f_{C37:3}$ denotes differential degradation factor between $C_{37:3}$ and $C_{37:2}$
869 alkenones.

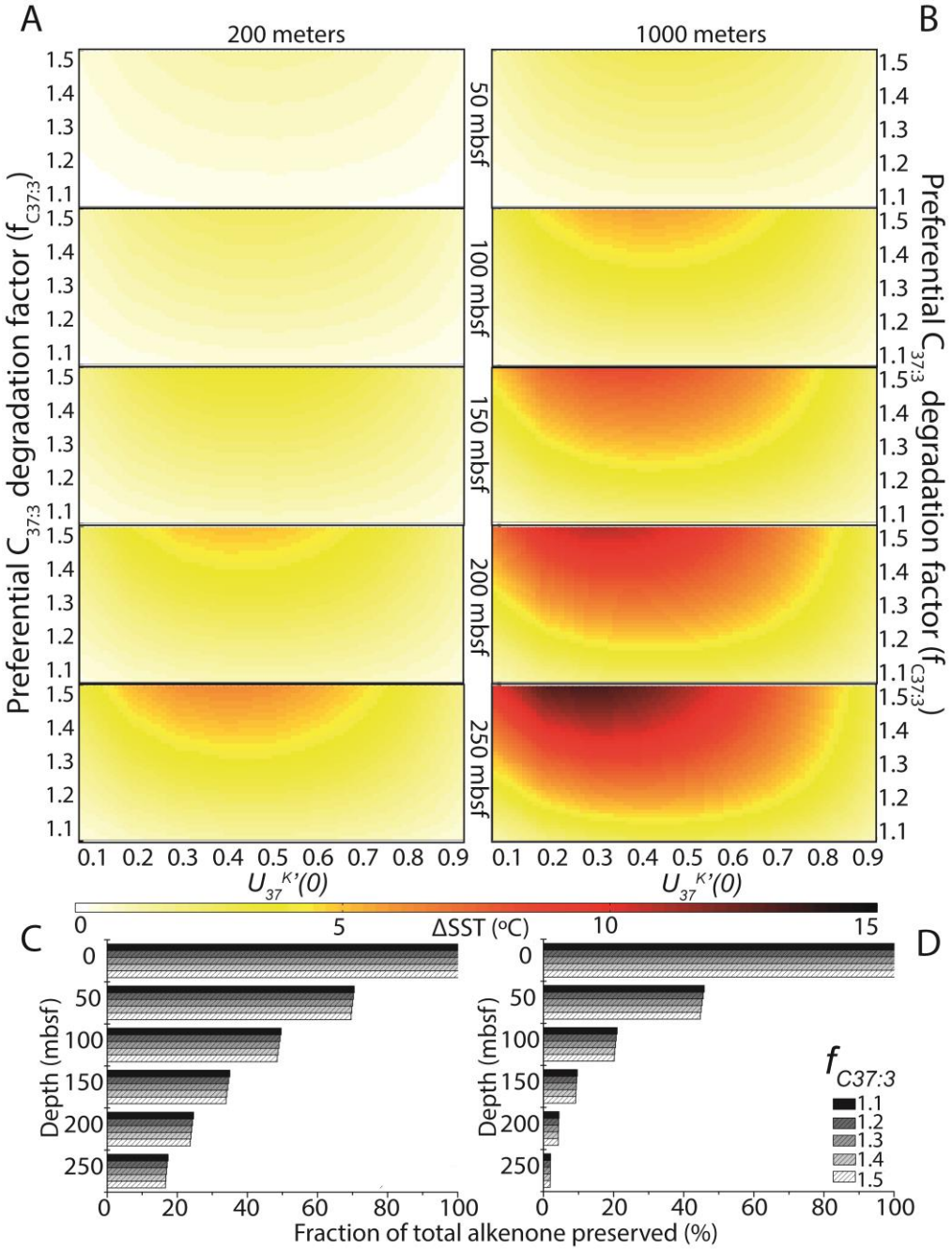

Figure 4. Interpolated SST positive bias and total alkenones preserved in sediment resulting from selective degradation of alkenones in a 1G-RTM simulation assuming a rate constant (k_i) of $2.5 \cdot 10^{-5}$ year^{-1}. (a) Downcore SST bias at 200 meters water depth; (b) Downcore SST bias at 1,000 meters water depth; (c) Downcore total alkenones preserved (%) in sediment at 200 meters water depth; (d) Downcore total alkenones preserved (%) in sediment at 1,000 meters water depth**.** ΔSST denotes SST at sediment-water interface (SWI) – SST at depth; $U_{37}^{K'}(0)$ denotes $U_{37}^{K'}$ initial values at SWI; $f_{C37:3}$ denotes differential degradation factor between $C_{37:3}$ and $C_{37:2}$ alkenones.

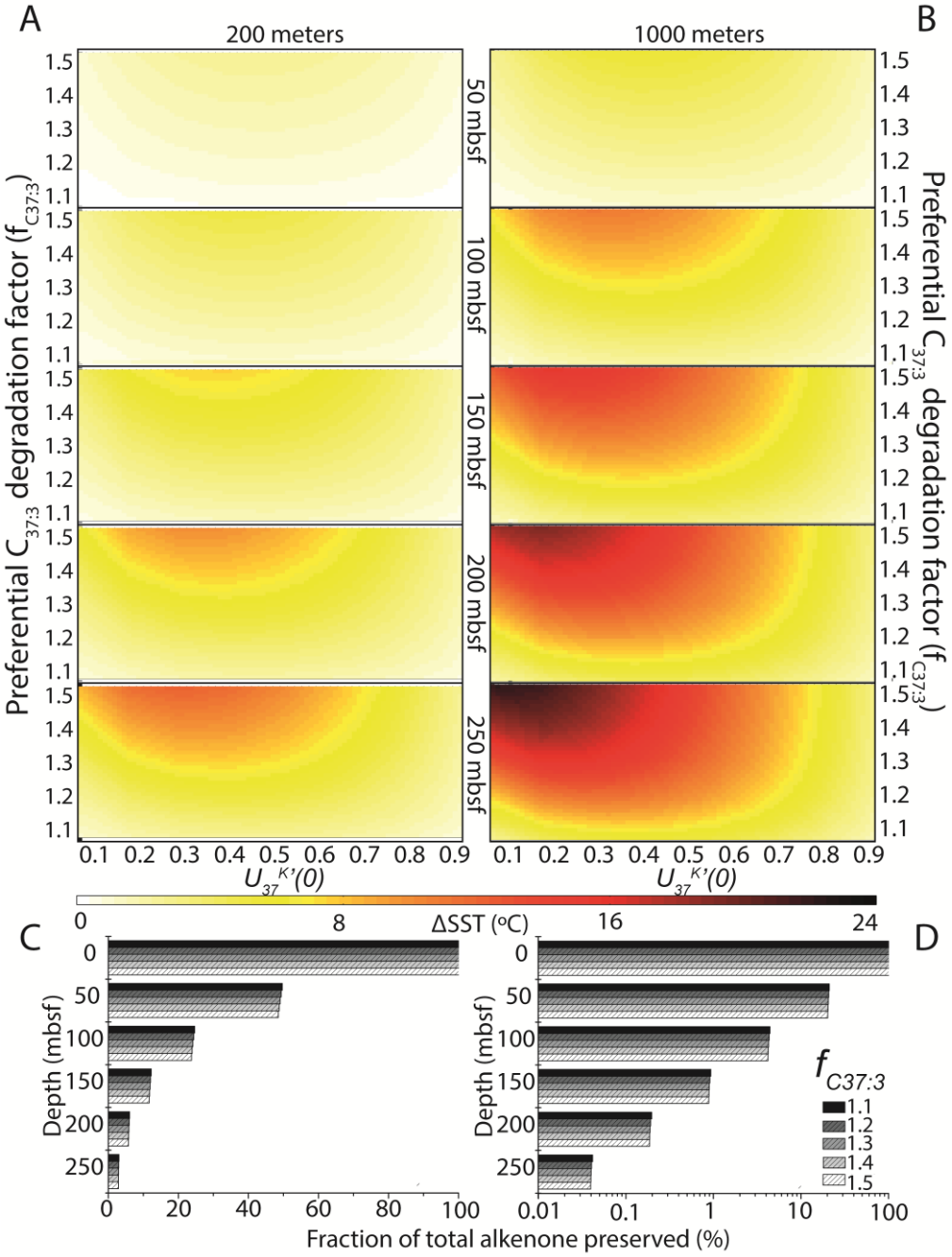

878

879 **Figure 5**. Interpolated SST positive bias and total alkenones preserved in sediment resulting from selective
880 degradation of alkenones in a 1G-RTM simulation assuming a rate constant (k_i) of $5.0 \cdot 10^{-5}$ year^{-1}. (a) Downcore
881 SST bias at 200 meters water depth; (b) Downcore SST bias at 1,000 meters water depth; (c) Downcore total
882 alkenones preserved (%) in sediment at 200 meters water depth; (d) Downcore total alkenones preserved (%) in
883 sediment at 1,000 meters water depth**.** ΔSST denotes SST at sediment-water interface (SWI) – SST at depth;
884 $U_{37}^{K'}(0)$ denotes $U_{37}^{K'}$ initial values at SWI; $f_{C37:3}$ denotes differential degradation factor between $C_{37:3}$ and $C_{37:2}$
885 alkenones.

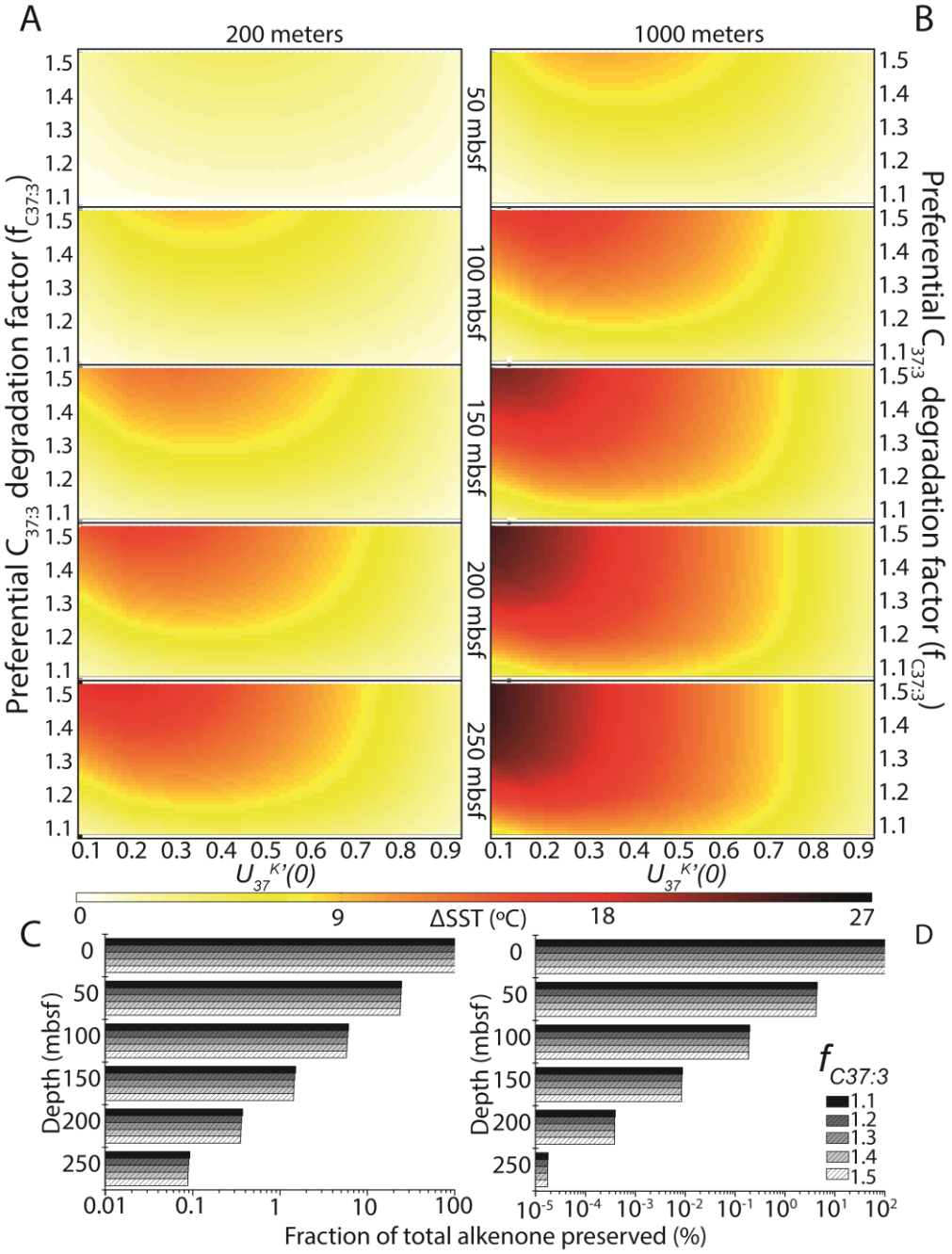

886

887 **Figure 6**. Interpolated SST positive bias interpolated plots and total alkenones preserved in sediment resulting
888 from selective degradation of alkenones in a 1G-RTM simulation assuming a rate constant (k_i) of $1.0 \cdot 10^{-4}$ year^{-1}. (a) Downcore SST bias at 200 meters water depth; (b) Downcore SST bias at 1,000 meters water depth; (c)
890 Downcore total alkenones preserved (%) in sediment at 200 meters water depth; (d) Downcore total alkenones
891 preserved (%) in sediment at 1,000 meters water depth**.** ΔSST denotes SST at sediment-water interface (SWI) –
892 SST at depth; $U_{37}^{K'}(0)$ denotes $U_{37}^{K'}$ initial values at SWI; $f_{C37:3}$ denotes differential degradation factor between
893 $C_{37:3}$ and $C_{37:2}$ alkenones.

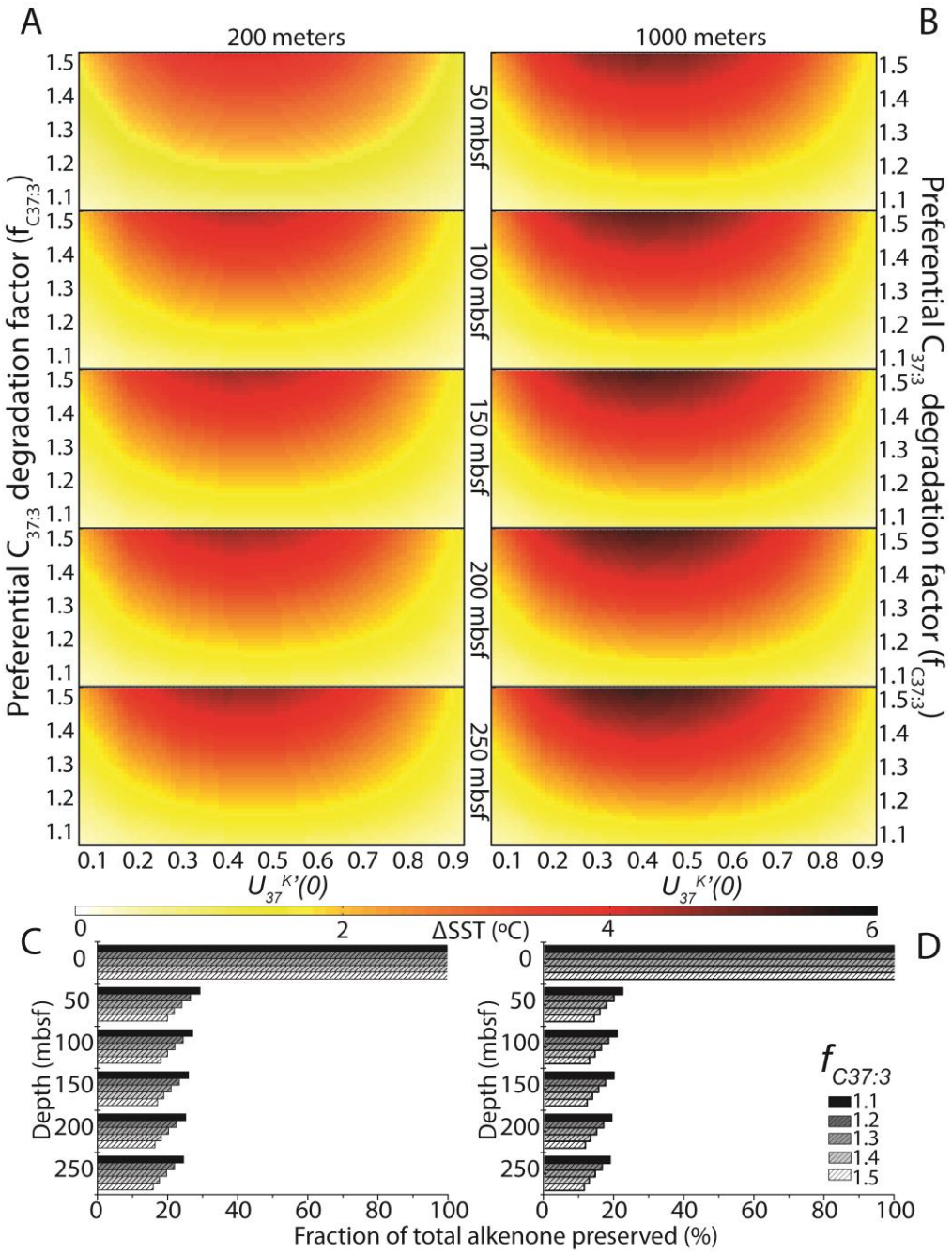

894

895 **Figure 7.** Interpolated SST positive bias and total alkenones preserved in sediment resulting from selective
896 degradation of alkenones in a RCM simulation assuming $pi = 10^{-1}$ and $a_i = 10^0$ years. (a) Downcore SST bias at
897 200 meters water depth; (b) Downcore SST bias at 1,000 meters water depth; (c) Downcore total alkenones
898 preserved (%) in sediment at 200 meters water depth; (d) Downcore total alkenones preserved (%) in sediment at
899 1,000 meters water depth**.** ΔSST denotes SST at sediment-water interface (SWI) – SST at depth; $U_{37}^{K'}(0)$ denotes
900 $U_{37}^{K'}$ initial values at SWI; $f_{C37:3}$ denotes differential degradation factor between $C_{37:3}$ and $C_{37:2}$ alkenones.

901

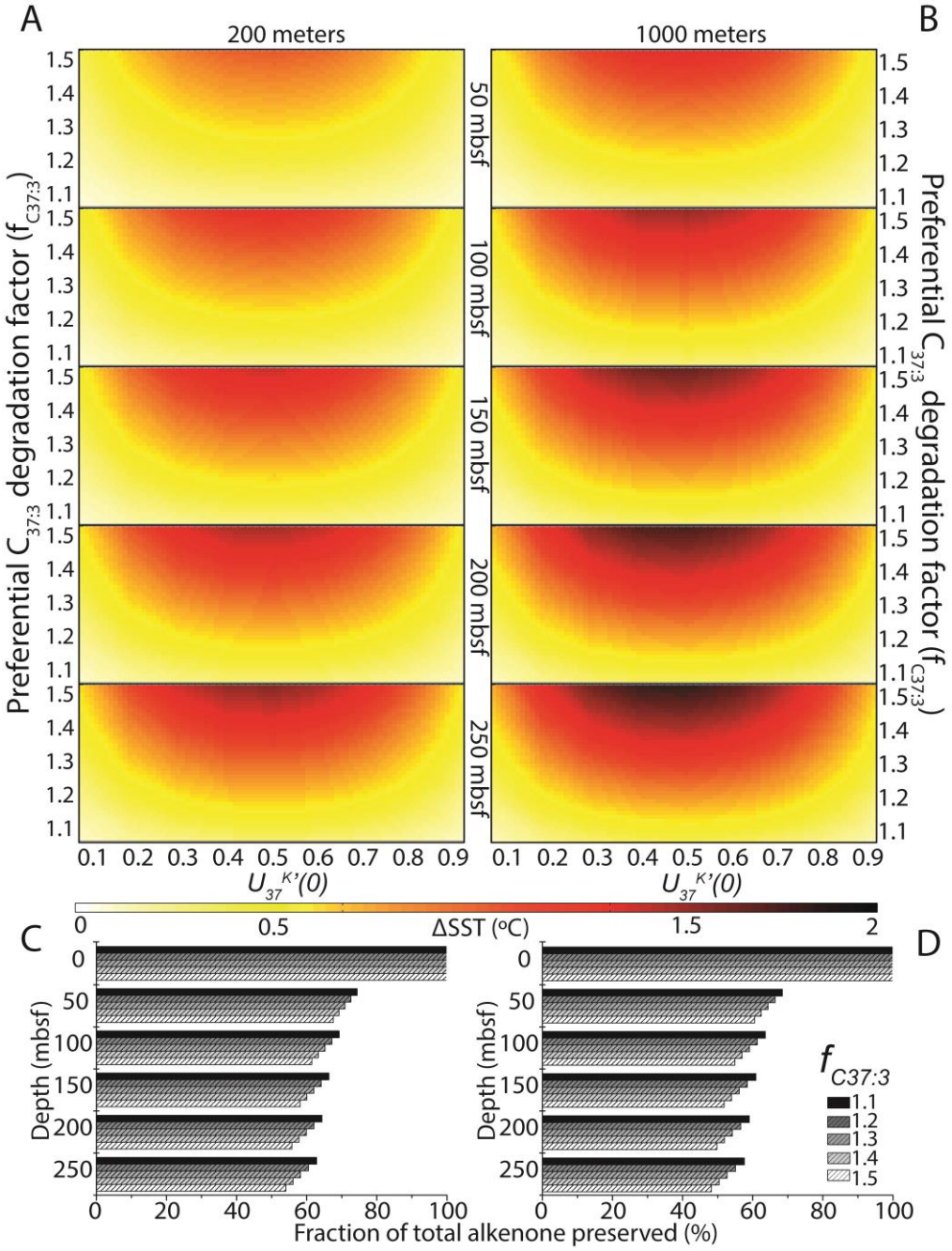

902

903 **Figure 8.** Interpolated SST positive bias and total alkenones preserved in sediment resulting from selective
904 degradation of alkenones in a RCM simulation assuming $pi = 10^{-1}$ and $a_i = 10^3$ years. (a) Downcore SST bias at
905 200 meters water depth; (b) Downcore SST bias at 1,000 meters water depth; (c) Downcore total alkenones
906 preserved (%) in sediment at 200 meters water depth; (d) Downcore total alkenones preserved (%) in sediment at
907 1,000 meters water depth**.** ΔSST denotes SST at sediment-water interface (SWI) – SST at depth; $U_{37}^{K'}(0)$ denotes
908 $U_{37}^{K'}$ initial values at SWI; $f_{C37:3}$ denotes differential degradation factor between $C_{37:3}$ and $C_{37:2}$ alkenones.

909

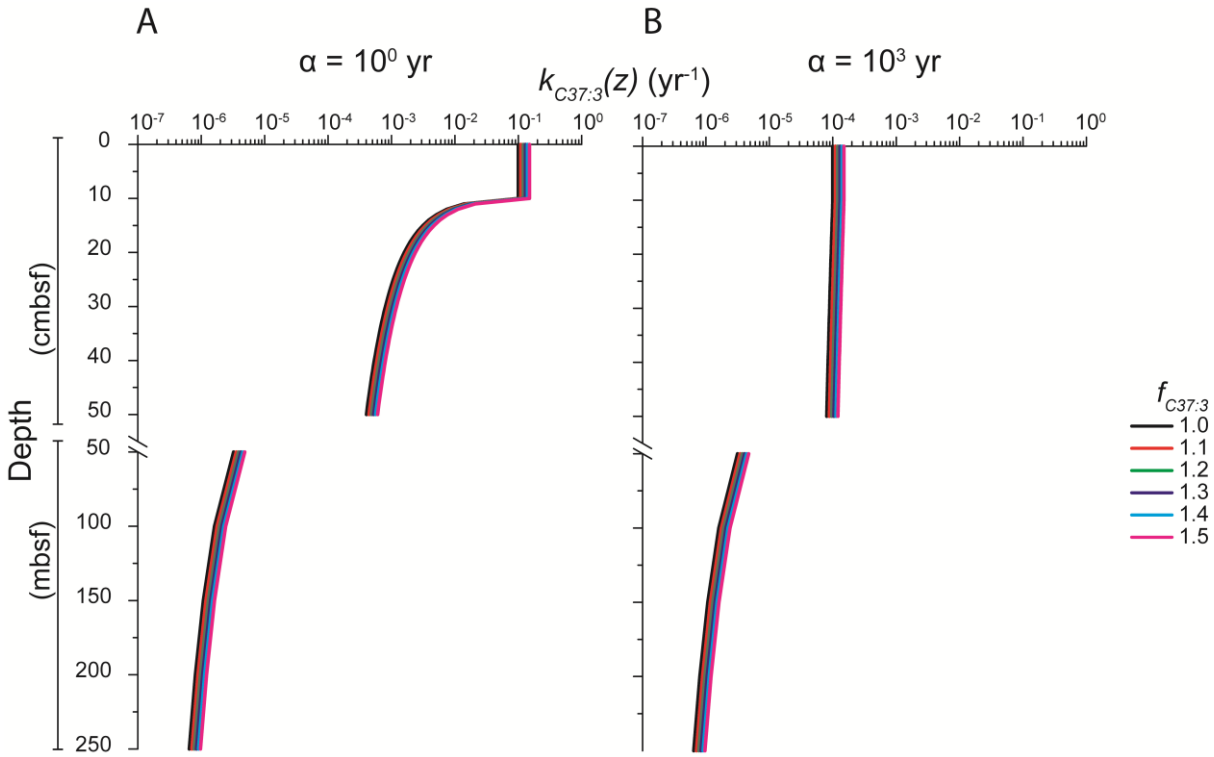

910

911 **Figure 9**. Simulated downcore changes in degradation rate constant $k_{C37:3}(z)$ assuming: p_i = 0.1; $U_{37}^{K'}(0)$ = 0.5. (a)
912 a_i = 10^0 years r; (b) a_i = 10^3 years; $f_{C37:3}$ ranges from 1.1 to 1.5 (colour lines); water depth = 1,000 meters. Note
913 the break in scale at y-axis: top layers represent the top 50 cmbsf where the most significant changes in $k_{C37:3}(z)$
914 and ΔSST take place; below the break, bottom layers represent the deeper sediment layers > 50 mbsf. The
915 discontinuity in the lines is due to the break in y-axis scale.

916

917

918

919

920

921

922

923

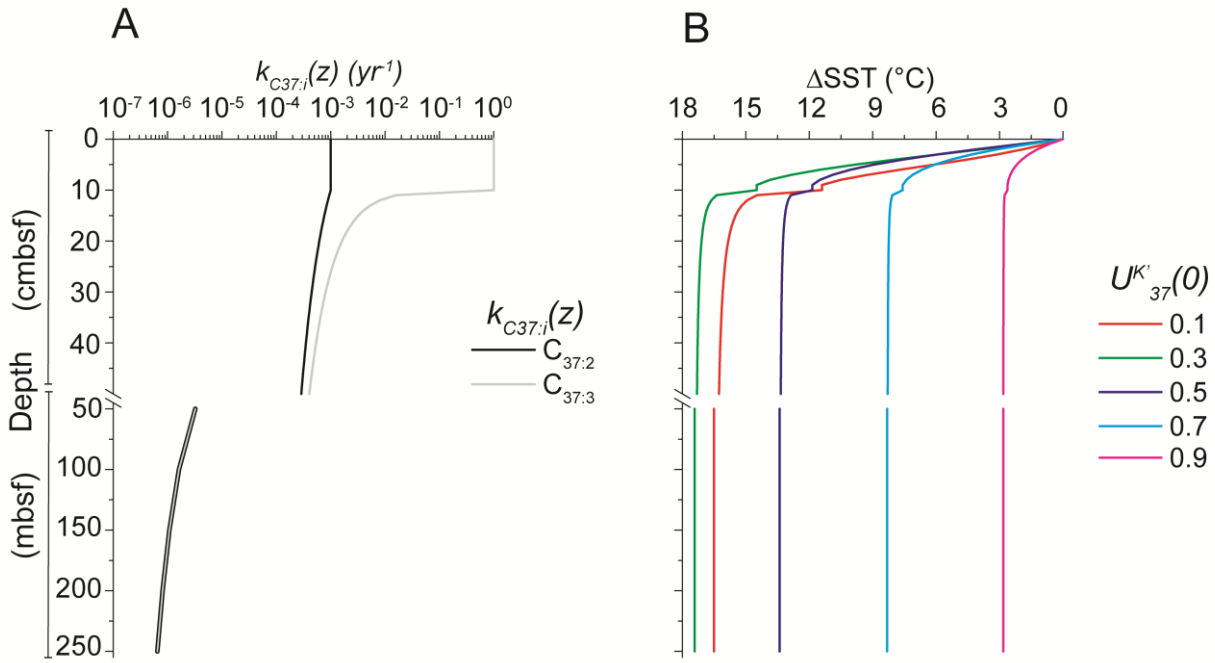

924

925 **Figure 10.** Simulated downcore changes in degradation rate constant $k_{C37:i}(z)$ ($C_{37:2}$ black line; $C_{37:3}$ grey line) (a)
926 and ΔSST (b) applying a power model scenario assuming: pi = 0.1; a_i = 100 years for $C_{37:2}$ (less labile pool of
927 alkenones); a_i = 0.1 years r for $C_{37:3}$ (more labile pool of alkenones); $U^{K'}_{37}(0)$ ranging from 0.1 to 0.9 (colour lines
928 in B); water depth = 1,000 meters. Note the break in scale at y-axis: top layers represent the top 50 cmbsf where
929 the most significant changes in $k_{C37:i}(z)$ and ΔSST take place; below the break, bottom layers represent the deeper
930 sediment layers > 50 mbsf. The discontinuity in the lines is due to the break in y-axis scale.

931

932

933

934

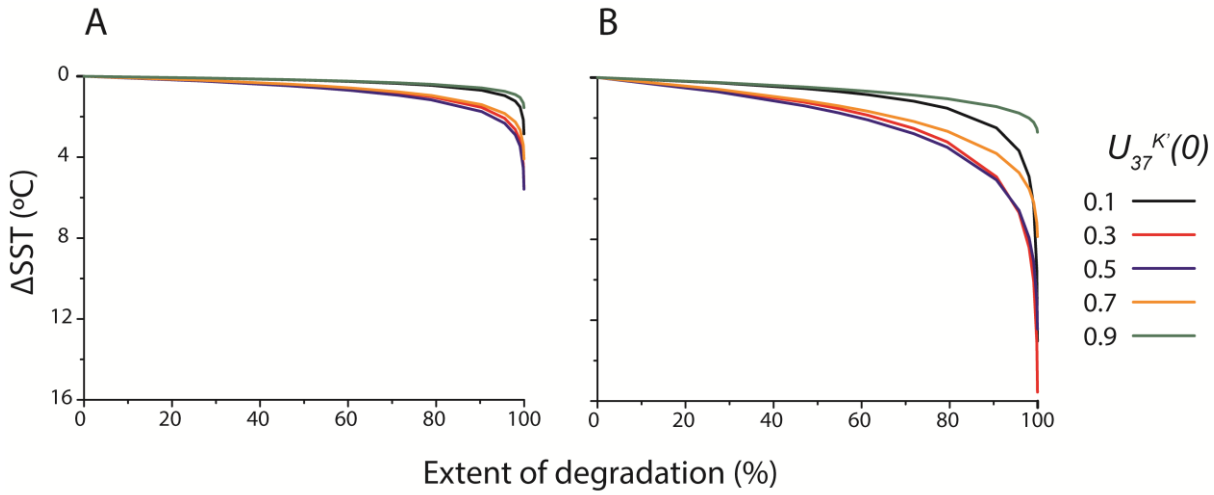

935

936 **Figure 11.** Increases in ΔSST with an increase in the extent of C_{37} alkenone degradation. Simulations assume: (a)

937 $f_{C37:3}$ = 1.1; (b) $f_{C37:3}$ = 1.3. Line colours represent $U_{37}^{K'}(0)$: black = 0.1; red = 0.3; blue = 0.5; yellow = 0.7; red =

938 0.9.

939

940

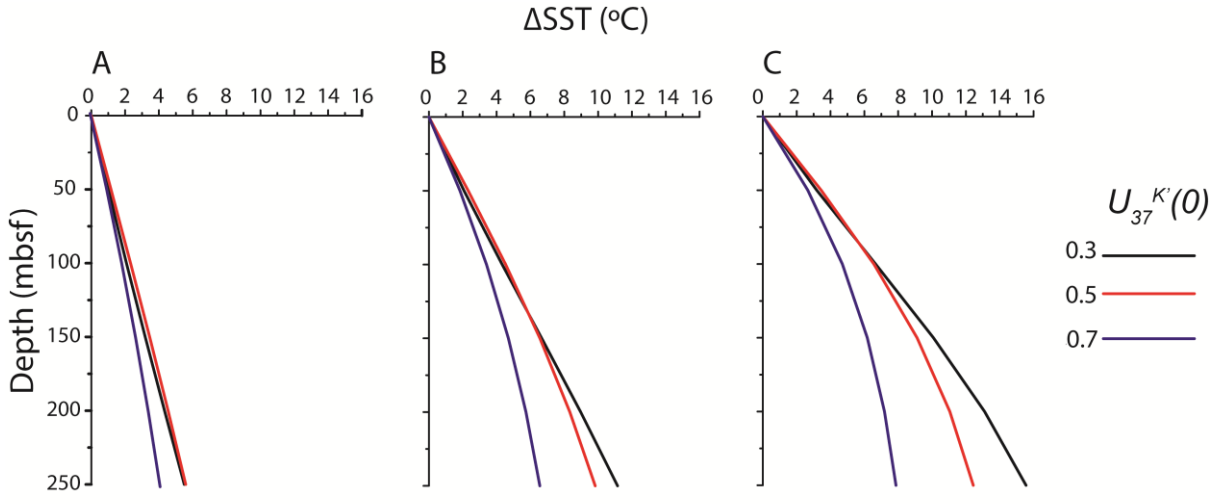

941

942 **Figure 12.** Increases in ΔSST with burial depth, assuming $k_i = 5 \cdot 10^{-5}$ year^{-1} and 1,000 meters water depth. (a)

943 $f_{C37:3}$ = 1.1; (b) $f_{C37:3}$ = 1.2; (c) $f_{C37:3}$ = 1.3. Line colours represent $U_{37}^{K'}(0)$: black = 0.3; red = 0.5; blue = 0.7.

944

945

946

947

Acknowledgements

FSF is supported by a PhD scholarship (grant number BEx 9541-13/6) from the Science without Borders Programme (Ciência sem Fronteiras), sponsored by the CAPES Foundation within Ministry of Education, Brazil. In addition, RDP acknowledges the advanced ERC grant 'The greenhouse earth system' (T-GRES, project reference 340923) and the Royal Society Wolfson Research Merit Award. SA acknowledges funding from the European Union's Horizon 2020 research and innovation programme under the Marie Sklodowska-Curie grant agreement number 643052 745 (C-CASCADES). The authors thank Dr Jack Middelburg, Dr Gordon Inglis, an anonymous reviewer, and the Associate Editor Liz Sikes for their constructive comments on this manuscript. The simulated data used in this research is available in tables and figures. The data derived from other studies is available in the cited references.

References

Aller, R. C. (1994), Bioturbation and remineralization of sedimentary organic matter: effects of redox oscillation, *Chem. Geol.*, *114*(3-4), 331–345, doi:10.1016/0009-2541(94)90062-0.

Aller, R. C., and N. E. Blair (2006), Carbon remineralization in the Amazon–Guianas tropical mobile mudbelt: A sedimentary incinerator, *Cont. Shelf Res.*, *26*(17-18), 2241–2259, doi:10.1016/j.csr.2006.07.016.

Arndt, S., B. B. Jørgensen, D. E. LaRowe, J. J. Middelburg, R. D. Pancost, and P. Regnier (2013), Quantifying the degradation of organic matter in marine sediments: A review and synthesis, *Earth-Sci. Rev.*, *123*, 53–86, doi:10.1016/j.earscirev.2013.02.008.

Arnosti, C. (2011), Microbial Extracellular Enzymes and the Marine Carbon Cycle, *Annu. Rev. Mar. Sci.*, *3*(1), 401–425, doi:10.1146/annurev-marine-120709-142731.

Bendle, J., and A. Rosell-Melé (2004), Distributions of U_{37}^{K} and $U_{37}^{K'}$ in the surface waters and sediments of the Nordic Seas: Implications for paleoceanography: distributions of U_{37}^{K} and $U_{37}^{K'}$, *Geochem. Geophys. Geosystems*, *5*(11), doi:10.1029/2004GC000741.

Benthien, A., and P. J. Müller (2000), Anomalously low alkenone temperatures caused by lateral particle and sediment transport in the Malvinas Current region, western Argentine Basin, *Deep Sea Res. Part Oceanogr. Res. Pap.*, *47*(12), 2369–2393, doi:10.1016/S0967-0637(00)00030-3.

Berner, R. A. (1980), *Early diagenesis: a theoretical approach*, Princeton series in geochemistry, Princeton University Press, Princeton, N.J.

Boon, J. J., P. J. W. van der Meer, J. W. Schuyl, J. W. de Leeuw, and P. A. Schenck (1978), Organic geochemical analyses of core samples from Site 362, Walvis Ridge, DSDP Leg 40, in *Initial Reports of the Deep Sea Drilling Project*, vol. 38/39/40/41.

Boudreau, B. P. (1986), Mathematics of tracer mixing in sediments; II, Nonlocal mixing and biological conveyor-belt phenomena, *Am. J. Sci.*, *286*(3), 199–238, doi:10.2475/ajs.286.3.199.

Boudreau, B. P. (1994), Is burial velocity a master parameter for bioturbation?, *Geochim. Cosmochim. Acta*, *58*(4), 1243–1249, doi:10.1016/0016-7037(94)90378-6.

Boudreau, B. P. (1997), *Diagenetic models and their implementation: modelling transport and reactions in aquatic sediments*, Springer, Berlin ; New York.

Boudreau, B. P. (1998), Mean mixed depth of sediments: The wherefore and the why, *Limnol. Oceanogr.*, *43*(3), 524–526, doi:10.4319/lo.1998.43.3.0524.

Boudreau, B. P., and B. R. Ruddick (1991), On a reactive continuum representation of organic matter diagenesis, *Am. J. Sci.*, *291*(5), 507–538, doi:10.2475/ajs.291.5.507.

Brassell, S. C. (2014), Climatic influences on the Paleogene evolution of alkenones, *Paleoceanography*, *29*(3), 255–272, doi:10.1002/2013PA002576.

1008 Brassell, S. C., and M. Dumitrescu (2004), Recognition of alkenones in a lower Aptian
1009 porcellanite from the west-central Pacific, *Org. Geochem.*, *35*(2), 181–188,
1010 doi:10.1016/j.orggeochem.2003.09.003.

1011 Brassell, S. C., G. Eglinton, I. T. Marlowe, U. Pflaumann, and M. Sarnthein (1986), Molecular
1012 stratigraphy: a new tool for climatic assessment, *Nature*, *320*(6058), 129–133,
1013 doi:10.1038/320129a0.

1014 Brinkhuis, H. et al. (2006), Episodic fresh surface waters in the Eocene Arctic Ocean, *Nature*,
1015 *441*(7093), 606–609, doi:10.1038/nature04692.

1016 Burdige, D. J. (2006), *Geochemistry of marine sediments*, Princeton University Press,
1017 Princeton, NJ.

1018 Castañeda, I. S., E. Schefuß, J. Pätzold, J. S. Sinninghe Damsté, S. Weldeab, and S. Schouten
1019 (2010), Millennial-scale sea surface temperature changes in the eastern Mediterranean
1020 (Nile River Delta region) over the last 27,000 years: Eastern Mediterranean SST
1021 records, *Paleoceanography*, *25*(1), doi:10.1029/2009PA001740.

1022 Conte, M. H., and G. Eglinton (1993), Alkenone and alkenoate distributions within the euphotic
1023 zone of the eastern North Atlantic: correlation with production temperature, *Deep Sea*
1024 *Res. Part Oceanogr. Res. Pap.*, *40*(10), 1935–1961, doi:10.1016/0967-0637(93)90040-
1025 A.

1026 Conte, M. H., G. Eglinton, and L. A. S. Madureira (1992), Long-chain alkenones and alkyl
1027 alkenoates as palaeotemperature indicators: their production, flux and early
1028 sedimentary diagenesis in the Eastern North Atlantic, *Org. Geochem.*, *19*(1-3), 287–
1029 298, doi:10.1016/0146-6380(92)90044-X.

1030 Cranwell, P. A., G. Eglinton, and N. Robinson (1987), Lipids of aquatic organisms as potential
1031 contributors to lacustrine sediments—II, *Org. Geochem.*, *11*(6), 513–527,
1032 doi:10.1016/0146-6380(87)90007-6.

1033 Farrimond, P., G. Eglinton, and S. C. Brassell (1986), Alkenones in Cretaceous black shales,
1034 Blake-Bahama Basin, western North Atlantic, *Org. Geochem.*, *10*(4-6), 897–903,
1035 doi:10.1016/S0146-6380(86)80027-4.

1036 Freeman, K. H., and S. G. Wakeham (1992), Variations in the distributions and isotopic
1037 composition of alkenones in Black Sea particles and sediments, *Org. Geochem.*, *19*(1-
1038 3), 277–285, doi:10.1016/0146-6380(92)90043-W.

1039 de Garidel-Thoron, T., Y. Rosenthal, L. Beaufort, E. Bard, C. Sonzogni, and A. C. Mix (2007),
1040 A multiproxy assessment of the western equatorial Pacific hydrography during the last
1041 30 kyr: deglacial equatorial pacific hydrography, *Paleoceanography*, *22*(3),
1042 doi:10.1029/2006PA001269.

1043 Gong, C., and D. J. Hollander (1999), Evidence for differential degradation of alkenones under
1044 contrasting bottom water oxygen conditions: implication for paleotemperature
1045 reconstruction, *Geochim. Cosmochim. Acta*, *63*(3-4), 405–411, doi:10.1016/S0016-
1046 7037(98)00283-X.

Grauel, A.-L., A. Leider, M.-L. S. Goudeau, I. A. Müller, S. M. Bernasconi, K.-U. Hinrichs, G. J. de Lange, K. A. F. Zonneveld, and G. J. M. Versteegh (2013), What do SST proxies really tell us? A high-resolution multiproxy ($U^{K'}_{37}$, TEX^{H}_{86} and foraminifera $\delta^{18}O$) study in the Gulf of Taranto, central Mediterranean Sea, *Quat. Sci. Rev.*, *73*, 115–131, doi:10.1016/j.quascirev.2013.05.007.

Grimalt, J. O., J. Rullkötter, M.-A. Sicre, R. Summons, J. Farrington, H. R. Harvey, M. Goñi, and K. Sawada (2000), Modifications of the C_{37} alkenone and alkenoate composition in the water column and sediment: Possible implications for sea surface temperature estimates in paleoceanography, *Geochem. Geophys. Geosystems*, *1*(11), doi:10.1029/2000GC000053.

Grimalt, J. O., E. Calvo, and C. Pelejero (2001), Sea surface paleotemperature errors in $U^{K'}_{37}$ estimation due to alkenone measurements near the limit of detection, *Paleoceanography*, *16*(2), 226–232, doi:10.1029/1999PA000440.

Herbert, T. D. (2001), Review of alkenone calibrations (culture, water column, and sediments), *Geochem. Geophys. Geosystems*, *2*(2), doi:10.1029/2000GC000055.

Hoefs, M. J. L., G. J. M. Versteegh, W. I. C. Rijpstra, J. W. de Leeuw, and J. S. S. Damsté (1998), Postdepositional oxic degradation of alkenones: Implications for the measurement of palaeo sea surface temperatures, *Paleoceanography*, *13*(1), 42–49, doi:10.1029/97PA02893.

Ho, S. L., and T. Laepple (2016), Flat meridional temperature gradient in the early Eocene in the subsurface rather than surface ocean, *Nat. Geosci.*, *9*(8), 606–610, doi:10.1038/ngeo2763.

Ho, S. L., B. D. A. Naafs, and F. Lamy (2013), Alkenone paleothermometry based in the Haptophyte Algae, in *The Encyclopedia of Quaternary Science*, vol. 2, pp. 755–764, Elselvier.

Huguet, C., J.-H. Kim, J. S. Sinninghe Damsté, and S. Schouten (2006), Reconstruction of sea surface temperature variations in the Arabian Sea over the last 23 kyr using organic proxies (TEX_{86} and $U^{K'}_{37}$): SST variations in the Arabian Sea, *Paleoceanography*, *21*(3), n/a–n/a, doi:10.1029/2005PA001215.

Huguet, C., J.-H. Kim, G. J. de Lange, J. S. Sinninghe Damsté, and S. Schouten (2009), Effects of long term oxic degradation on the TEX_{86} and BIT organic proxies, *Org. Geochem.*, *40*(12), 1188–1194, doi:10.1016/j.orggeochem.2009.09.003.

Huguet, C., B. Martrat, J. O. Grimalt, J. S. Sinninghe Damsté, and S. Schouten (2011), Coherent millennial-scale patterns in $U^{K'}_{37}$ and $TEX_{86}{}^{H}$ temperature records during the penultimate interglacial-to-glacial cycle in the western Mediterranean: $U^{K'}_{37}$ and $TEX_{86}{}^{H}$ paleothermometry, *Paleoceanography*, *26*(2), doi:10.1029/2010PA002048.

Keil, R. G., A. F. Dickens, T. Arnarson, B. L. Nunn, and A. H. Devol (2004), What is the oxygen exposure time of laterally transported organic matter along the Washington margin?, *Mar. Chem.*, *92*(1-4), 157–165, doi:10.1016/j.marchem.2004.06.024.

1086 de Leeuw, J. W., F. W. v.d. Meer, W. I. C. Rijpstra, and P. A. Schenck (1980), On the
1087 occurrence and structural identification of long chain unsaturated ketones and
1088 hydrocarbons in sediments, *Phys. Chem. Earth*, *12*, 211–217, doi:10.1016/0079-
1089 1946(79)90105-8.

1090 Li, D., M. Zhao, J. Tian, and L. Li (2013), Comparison and implication of TEX86 and U37K'
1091 temperature records over the last 356kyr of ODP Site 1147 from the northern South
1092 China Sea, *Palaeogeogr. Palaeoclimatol. Palaeoecol.*, *376*, 213–223,
1093 doi:10.1016/j.palaeo.2013.02.031.

1094 Liu, Z., M. Pagani, D. Zinniker, R. DeConto, M. Huber, H. Brinkhuis, S. R. Shah, R. M. Leckie,
1095 and A. Pearson (2009), Global Cooling During the Eocene-Oligocene Climate
1096 Transition, *Science*, *323*(5918), 1187–1190, doi:10.1126/science.1166368.

1097 Lopes dos Santos, R. A., M. Prange, I. S. Castañeda, E. Schefuß, S. Mulitza, M. Schulz, E. M.
1098 Niedermeyer, J. S. Sinninghe Damsté, and S. Schouten (2010), Glacial–interglacial
1099 variability in Atlantic meridional overturning circulation and thermocline adjustments
1100 in the tropical North Atlantic, *Earth Planet. Sci. Lett.*, *300*(3-4), 407–414,
1101 doi:10.1016/j.epsl.2010.10.030.

1102 Lyle, M., F. G. Prahl, and M. A. Sparrow (2006), Data report: Reconnaissence of organic
1103 biomarkers in Leg 199 sediments, in *Proceedings of the Ocean Drilling Program,*
1104 *Scientific Results*.

1105 Madureira, L. A. S., M. H. Conte, and G. Eglinton (1995), Early diagenesis of lipid biomarker
1106 compounds in North Atlantic sediments, *Paleoceanography*, *10*(3), 627–642,
1107 doi:10.1029/94PA03299.

1108 Marlowe, I. T., S. C. Brassell, G. Eglinton, and J. C. Green (1984), Long chain unsaturated
1109 ketones and esters in living algae and marine sediments, *Org. Geochem.*, *6*, 135–141,
1110 doi:10.1016/0146-6380(84)90034-2.

1111 Marlowe, I. T., S. C. Brassell, G. Eglinton, and J. C. Green (1990), Long-chain alkenones and
1112 alkyl alkenoates and the fossil coccolith record of marine sediments, *Chem. Geol.*, *88*(3-
1113 4), 349–375, doi:10.1016/0009-2541(90)90098-R.

1114 Mayer, L. M. (1995), Sedimentary organic matter preservation: an assessment and speculative
1115 synthesis—a comment, *Mar. Chem.*, *49*(2-3), 123–126, doi:10.1016/0304-
1116 4203(95)00011-F.

1117 McCaffrey, M. A., J. W. Farrington, and D. J. Repeta (1990), The organic geochemistry of
1118 Peru margin surface sediments: I. A comparison of the C37 alkenone and historical El
1119 Niño records, *Geochim. Cosmochim. Acta*, *54*(6), 1671–1682, doi:10.1016/0016-
1120 7037(90)90399-6.

1121 McClymont, E. L., R. S. Ganeshram, L. E. Pichevin, H. M. Talbot, B. E. van Dongen, R. C.
1122 Thunell, A. M. Haywood, J. S. Singarayer, and P. J. Valdes (2012), Sea-surface
1123 temperature records of Termination 1 in the Gulf of California: Challenges for seasonal
1124 and interannual analogues of tropical Pacific climate change: Gulf of California
1125 Termination 1, *Paleoceanography*, *27*(2), doi:10.1029/2011PA002226.

Mercer, J. L., and M. Zhao (2004), Alkenone stratigraphy on the Northern South China Sea for the past 35 m.y., sites 1147 and 1148, ODP Leg 181, in *Proceedings of the Ocean Drilling Program, Scientific Results*, vol. 184.

Middelburg, J. J. (1989), A simple rate model for organic matter decomposition in marine sediments, *Geochim. Cosmochim. Acta*, *53*(7), 1577–1581, doi:10.1016/0016-7037(89)90239-1.

Middelburg, J. J., K. Soetaert, and P. M. J. Herman (1997), Empirical relationships for use in global diagenetic models, *Deep Sea Res. Part Oceanogr. Res. Pap.*, *44*(2), 327–344, doi:10.1016/S0967-0637(96)00101-X.

Mollenhauer, G., T. . Eglinton, N. Ohkouchi, R. . Schneider, P. . Müller, P. . Grootes, and J. Rullkötter (2003), Asynchronous alkenone and foraminifera records from the Benguela Upwelling System, *Geochim. Cosmochim. Acta*, *67*(12), 2157–2171, doi:10.1016/S0016-7037(03)00168-6.

Müller, P. J., and G. Fischer (2001), A 4-year sediment trap record of alkenones from the filamentous upwelling region off Cape Blanc, NW Africa and a comparison with distributions in underlying sediments, *Deep Sea Res. Part Oceanogr. Res. Pap.*, *48*(8), 1877–1903, doi:10.1016/S0967-0637(00)00109-6.

Müller, P. J., G. Kirst, G. Ruhland, I. von Storch, and A. Rosell-Melé (1998), Calibration of the alkenone paleotemperature index $U_{37}^{K'}$ based on core-tops from the eastern South Atlantic and the global ocean (60°N-60°S), *Geochim. Cosmochim. Acta*, *62*(10), 1757–1772, doi:10.1016/S0016-7037(98)00097-0.

Ohkouchi, N., T. I. Eglinton, L. D. Keigwin, and J. . Hayes (2002), Spatial and Temporal Offsets Between Proxy Records in a Sediment Drift, *Science*, *298*(5596), 1224–1227, doi:10.1126/science.1075287.

Pagani, M., M. A. Arthur, and K. H. Freeman (1999), Miocene evolution of atmospheric carbon dioxide, *Paleoceanography*, *14*(3), 273–292, doi:10.1029/1999PA900006.

Pagani, M., M. A. Arthur, and K. H. Freeman (2000), Variations in Miocene phytoplankton growth rates in the southwest Atlantic: Evidence for changes in ocean circulation, *Paleoceanography*, *15*(5), 486–496, doi:10.1029/1999PA000484.

Pagani, M., J. C. Zachos, K. H. Freeman, B. Tipple, and S. Bohaty (2005), Marked Decline in Atmospheric Carbon Dioxide Concentrations During the Paleogene, *Science*, *309*(5734), 600–603, doi:10.1126/science.1110063.

Pagani, M., Z. Liu, J. LaRiviere, and A. C. Ravelo (2010), High Earth-system climate sensitivity determined from Pliocene carbon dioxide concentrations, *Nat. Geosci.*, *3*(1), 27–30, doi:10.1038/ngeo724.

Pearson, P. N., P. W. Ditchfield, J. Singano, K. G. Harcourt-Brown, C. J. Nicholas, R. K. Olsson, N. J. Shackleton, and M. A. Hall (2001), Warm tropical sea surface temperatures in the Late Cretaceous and Eocene epochs, *Nature*, *413*(6855), 481–487, doi:10.1038/35097000.

Pearson, P. N., B. E. van Dongen, C. J. Nicholas, R. D. Pancost, S. Schouten, J. M. Singano, and B. S. Wade (2007), Stable warm tropical climate through the Eocene Epoch, *Geology*, *35*(3), 211, doi:10.1130/G23175A.1.

Prahl, F., T. Herbert, S. C. Brassell, N. Ohkouchi, M. Pagani, D. Repeta, A. Rosell-Melé, and E. Sikes (2000), Status of alkenone paleothermometer calibration: Report from Working Group 3: paleothermometer calibration, *Geochem. Geophys. Geosystems*, *1*(11), doi:10.1029/2000GC000058.

Prahl, F. ., C. . Pilskaln, and M. . Sparrow (2001), Seasonal record for alkenones in sedimentary particles from the Gulf of Maine, *Deep Sea Res. Part Oceanogr. Res. Pap.*, *48*(2), 515–528, doi:10.1016/S0967-0637(00)00057-1.

Prahl, F. G., and S. G. Wakeham (1987), Calibration of unsaturation patterns in long-chain ketone compositions for palaeotemperature assessment, *Nature*, *330*(6146), 367–369, doi:10.1038/330367a0.

Prahl, F. G., L. A. Muehlhausen, and D. L. Zahnle (1988), Further evaluation of long-chain alkenones as indicators of paleoceanographic conditions, *Geochim. Cosmochim. Acta*, *52*(9), 2303–2310, doi:10.1016/0016-7037(88)90132-9.

Prahl, F. G., G. J. de Lange, M. Lyle, and M. A. Sparrow (1989), Post-depositional stability of long-chain alkenones under contrasting redox conditions, *Nature*, *341*(6241), 434–437, doi:10.1038/341434a0.

Prahl, F. G., G. L. Cowie, G. J. De Lange, and M. A. Sparrow (2003), Selective organic matter preservation in "burn-down" turbidites on the Madeira Abyssal Plain: selective preservation, *Paleoceanography*, *18*(2), doi:10.1029/2002PA000853.

Rechka, J. A., and J. R. Maxwell (1988), Characterisation of alkenone temperature indicators in sediments and organisms, *Org. Geochem.*, *13*(4-6), 727–734, doi:10.1016/0146-6380(88)90094-0.

Rodrigo-Gámiz, M., S. W. Rampen, S. Schouten, and J. S. Sinninghe Damsté (2016), The impact of oxic degradation on long chain alkyl diol distributions in Arabian Sea surface sediments, *Org. Geochem.*, *100*, 1–9, doi:10.1016/j.orggeochem.2016.07.003.

Rontani, J.-F., and S. G. Wakeham (2008), Alteration of alkenone unsaturation ratio with depth in the Black Sea: Potential roles of stereomutation and aerobic biodegradation, *Org. Geochem.*, *39*(9), 1259–1268, doi:10.1016/j.orggeochem.2008.06.002.

Rontani, J.-F., P. Cuny, V. Grossi, and B. Beker (1997), Stability of long-chain alkenones in senescing cells of Emiliania huxleyi: effect of photochemical and aerobic microbial degradation on the alkenone unsaturation ratio ($U_{37}^{K'}$), *Org. Geochem.*, *26*(7-8), 503–509, doi:10.1016/S0146-6380(97)00023-5.

Rontani, J.-F., P. Bonin, I. Jameson, and J. K. Volkman (2005), Degradation of alkenones and related compounds during oxic and anoxic incubation of the marine haptophyte Emiliania huxleyi with bacterial consortia isolated from microbial mats from the Camargue, France, *Org. Geochem.*, *36*(4), 603–618, doi:10.1016/j.orggeochem.2004.10.010.

Rontani, J.-F., R. Harji, S. Guasco, F. G. Prahl, J. K. Volkman, N. B. Bhosle, and P. Bonin (2008), Degradation of alkenones by aerobic heterotrophic bacteria: Selective or not?, *Org. Geochem.*, *39*(1), 34–51, doi:10.1016/j.orggeochem.2007.10.003.

Rontani, J.-F., J. K. Volkman, F. G. Prahl, and S. G. Wakeham (2013), Biotic and abiotic degradation of alkenones and implications for paleoproxy applications: A review, *Org. Geochem.*, *59*, 95–113, doi:10.1016/j.orggeochem.2013.04.005.

Rosell-Melé, A., J. Carter, and G. Eglinton (1994), Distributions of long-chain alkenones and alkyl alkenoates in marine surface sediments from the North East Atlantic, *Org. Geochem.*, *22*(3-5), 501–509, doi:10.1016/0146-6380(94)90122-8.

Schouten, S., E. C. Hopmans, E. Schefuß, and J. S. Sinninghe Damsté (2002), Distributional variations in marine crenarchaeotal membrane lipids: a new tool for reconstructing ancient sea water temperatures?, *Earth Planet. Sci. Lett.*, *204*(1-2), 265–274, doi:10.1016/S0012-821X(02)00979-2.

Schouten, S., J. J. Middelburg, E. C. Hopmans, and J. S. Sinninghe Damsté (2010), Fossilization and degradation of intact polar lipids in deep subsurface sediments: A theoretical approach, *Geochim. Cosmochim. Acta*, *74*(13), 3806–3814, doi:10.1016/j.gca.2010.03.029.

Schouten, S., E. C. Hopmans, and J. S. Sinninghe Damsté (2013), The organic geochemistry of glycerol dialkyl glycerol tetraether lipids: A review, *Org. Geochem.*, *54*, 19–61, doi:10.1016/j.orggeochem.2012.09.006.

Seki, O., D. N. Schmidt, S. Schouten, E. C. Hopmans, J. S. Sinninghe Damsté, and R. D. Pancost (2012), Paleoceanographic changes in the Eastern Equatorial Pacific over the last 10 Myr: paleoceanography over the past 10 myr, *Paleoceanography*, *27*(3), doi:10.1029/2011PA002158.

Sikes, E. L., and M.-A. Sicre (2002), Relationship of the tetra-unsaturated C_{37} alkenone to salinity and temperature: Implications for paleoproxy applications: tetra-unsaturated C_{37} alkenone, *Geochem. Geophys. Geosystems*, *3*(11), 1–11, doi:10.1029/2002GC000345.

Sikes, E. L., J. W. Farrington, and L. D. Keigwin (1991), Use of the alkenone unsaturation ratio U_{37}^{K} to determine past sea surface temperatures: core-top SST calibrations and methodology considerations, *Earth Planet. Sci. Lett.*, *104*(1), 36–47, doi:10.1016/0012-821X(91)90235-A.

Sikes, E. L., J. K. Volkman, L. G. Robertson, and J.-J. Pichon (1997), Alkenones and alkenes in surface waters and sediments of the Southern Ocean: Implications for paleotemperature estimation in polar regions, *Geochim. Cosmochim. Acta*, *61*(7), 1495–1505, doi:10.1016/S0016-7037(97)00017-3.

Sun, M.-Y., and S. G. Wakeham (1994), Molecular evidence for degradation and preservation of organic matter in the anoxic Black Sea Basin, *Geochim. Cosmochim. Acta*, *58*(16), 3395–3406, doi:10.1016/0016-7037(94)90094-9.

Teece, M. A., J. M. Getliff, J. W. Leftley, R. J. Parkes, and J. R. Maxwell (1998), Microbial degradation of the marine prymnesiophyte Emiliania huxleyi under oxic and anoxic conditions as a model for early diagenesis: long chain alkadienes, alkenones and alkyl alkenoates, *Org. Geochem.*, *29*(4), 863–880, doi:10.1016/S0146-6380(98)00145-4.

Volkman, J. K. (2000), Ecological and environmental factors affecting alkenone distributions in seawater and sediments: review, *Geochem. Geophys. Geosystems*, *1*(9), doi:10.1029/2000GC000061.

Volkman, J. K., G. Eglinton, E. D. S. Corner, and T. E. V. Forsberg (1980a), Long-chain alkenes and alkenones in the marine coccolithophorid Emiliania huxleyi, *Phytochemistry*, *19*(12), 2619–2622, doi:10.1016/S0031-9422(00)83930-8.

Volkman, J. K., G. Eglinton, E. D. S. Corner, and J. R. Sargent (1980b), Novel unsaturated straight-chain C_{37} - C_{39} methyl and ethyl ketones in marine sediments and a coccolithophore Emiliania huxleyi, *Phys. Chem. Earth*, *12*, 219–227, doi:10.1016/0079-1946(79)90106-X.

Volkman, J. K., J. W. Farrinton, R. B. Gagosian, and S. G. Wakeham (1983), Lipid composition of coastal marine sediments from Peru Upwelling Region, in *Advances in organic geochemistry, 1981: proceedings of the 10th International Meeting on Organic Geochemistry, University of Bergen, Norway, 14-18 September 1981*, p. 800, Wiley, Chichester ; New York.

Volkman, J. K., S. M. Barrerr, S. I. Blackburn, and E. L. Sikes (1995), Alkenones in Gephyrocapsa oceanica: Implications for studies of paleoclimate, *Geochim. Cosmochim. Acta*, *59*(3), 513–520, doi:10.1016/0016-7037(95)00325-T.

Weller, P., and R. Stein (2008), Paleogene biomarker records from the central Arctic Ocean (Integrated Ocean Drilling Program Expedition 302): Organic carbon sources, anoxia, and sea surface temperature: Paleogene Central Arctic Ocean biomarker, *Paleoceanography*, *23*(1), doi:10.1029/2007PA001472.

Zabeti, N., P. Bonin, J. K. Volkman, I. D. Jameson, S. Guasco, and J.-F. Rontani (2010), Potential alteration of $U_{37}^{K'}$ paleothermometer due to selective degradation of alkenones by marine bacteria isolated from the haptophyte Emiliania huxleyi: Isolation of alkenone-degrading bacteria from E. huxleyi, *FEMS Microbiol. Ecol.*, doi:10.1111/j.1574-6941.2010.00885.x.

Zonneveld, K. A. F. et al. (2010), Selective preservation of organic matter in marine environments; processes and impact on the sedimentary record, *Biogeosciences*, *7*(2), 483–511, doi:10.5194/bg-7-483-2010.